Journal of Environmental Chemical Engineering 14 (2026) 122861

Contents lists available at ScienceDirect

Journal of Environmental Chemical Engineering

journal homepage: www.elsevier.com/locate/jece

Chemical looping combustion of the aqueous phase fraction of bio-oil from biomass pyrolysis

César Gracia-Monforte *, Alejandro Lete, Javier Ábrego, Jesús Arauzo

Thermochemical Processes Group (GPT), Aragon Institute for Engineering Research (I3A), University of Zaragoza, Zaragoza 50018, Spain

ARTICLE INFO

Keywords:
Chemical Looping Combustion (CLC)
Bio-oil
Carbon capture
Oxygen carrier
Biomass valorization
Pyrolysis

ABSTRACT

The aqueous fraction of pyrolysis bio-oil, which can account for up to 85 wt% water, is typically considered a low-value by-product due to its high water content, corrosivity, toxicity, and low heating value. Its effective utilization remains a challenge for the development of sustainable biomass valorization technologies. In this work, the potential of chemical looping combustion (CLC) was evaluated as an alternative route for converting this fraction into energy while enabling inherent CO_2 capture. Several oxygen carriers (OCs) based on Cu, Fe, Ni, and Mn were screened in a fixed-bed reactor at 650 °C using a synthetic model mixture representative of the aqueous bio-oil fraction (acetone, acetic acid, phenol, p-cresol, and 2-butanone). The laboratory-synthesized CuO/Al_2O_3 powder OC exhibited the best performance, achieving complete oxidation of the mixture to CO_2 and H_2O without detectable by-products during the combustion phase. Furthermore, the selected OC demonstrated highly stable redox performance and regenerability over multiple cycles at 650 and 750 °C, with the operation at 750 °C effectively minimizing carbon deposition compared to 650 °C. Overall, this low-temperature CLC approach with a CuO/Al_2O_3 carrier successfully addresses prior challenges of severe carbon deposition and oxygen carrier deactivation, providing a robust pathway for aqueous bio-oil valorization.

1. Introduction

The transition towards sustainable energy systems is driven by the urgent need to reduce greenhouse gas (GHG) emissions, mitigate climate change, and decrease dependence on fossil fuels. Biomass pyrolysis has emerged as a promising thermochemical conversion pathway for producing renewable fuels and chemicals, owing to its ability to convert lignocellulosic biomass into bio-oil, syngas, and biochar [1]. Among these products, bio-oil has attracted considerable attention as a potential substitute for fossil-based fuels, since they are composed of hydrocarbons, which gives them considerable calorific value, and they come from a renewable energy source. However, raw bio-oil is a highly complex mixture with properties such as high oxygen content, acidity, and poor stability that limit its direct application in combustion engines or power generation systems [2]. Furthermore, a critical challenge lies in the valorization of bio-oil, which can account for up to 30 wt% water of the total liquid product [3].

Bio-oil obtained in fast pyrolysis typically yields 50–75 wt% [4,5], while in slow pyrolysis produces significantly lower liquid yields 30–45 wt% [6], with a higher proportion of char and gas due to longer residence times and lower heating rates. Bio-oil derived from biomass pyrolysis can undergo spontaneous phase separation into a water-rich aqueous fraction and a heavier organic fraction [7,8]. The aqueous phase typically contains a very high proportion of water, normally exceeding 50 wt% and is dominated by light oxygenated compounds such as acids, ketones and aldehydes [7]. In contrast, the organic phase contains significantly lower water content and is enriched in higher-molecular-weight oxygenated compounds and phenolics [8], reflecting the compositional contrast and different potential utilization pathways of both fractions. The high-water content in the aqueous fraction results in a low heating value, making conventional combustion or upgrading strategies unattractive [4]. Consequently, the aqueous phase is often considered a low-value by-product, despite its significant share of the pyrolysis yield. While fast pyrolysis typically yields up to 75 wt% of total bio-oil, the aqueous fraction can represent between 60 and 70 wt% of this liquid product [4,9], depending on the biomass source and process conditions. This fraction is mainly composed of water (20–30 wt%) and a complex mixture of water-soluble organics. Developing efficient strategies for its utilization is therefore crucial to improving the overall economics and sustainability of biomass pyrolysis.

* Corresponding author.
E-mail address: c.gracia@unizar.es (C. Gracia-Monforte).

https://doi.org/10.1016/j.jece.2026.122861
Received 11 March 2026; Received in revised form 17 April 2026; Accepted 24 April 2026
Available online 26 April 2026

Moreover, the aqueous fraction is known to contain a wide range of toxic and corrosive oxygenated compounds, which pose environmental concerns and require dedicated treatment prior to disposal. Its direct valorization would therefore not only improve process efficiency but also significantly reduce the environmental burden associated with wastewater management, contributing to a more sustainable and integrated biomass conversion process [4,10,11].

Chemical looping combustion (CLC) represents an advanced combustion technology with inherent CO_2 capture, which could offer a viable route for the utilization of the aqueous bio-oil fraction. In CLC, fuel oxidation is driven by oxygen transfer from a solid oxygen carrier (OC)-generally a metal oxide- thereby eliminating direct fuel–air contact. The OC is subsequently regenerated with air, releasing N_2 and unused O_2. As a result, the flue gas from the fuel reactor consists almost exclusively of CO_2 and H_2O, from which pure CO_2 can be easily separated after condensation [12]. This process not only enables efficient combustion but also provides a cost-effective solution for carbon capture, avoiding the high energy penalties associated with post-combustion capture methods [13,14].

Over the past two decades, extensive research has been conducted on CLC with gaseous fuels, such as methane and syngas, demonstrating high efficiency and stable operation [15–17]. CLC of solid fuels such as coal and biomass has also been investigated, though it presents additional challenges due to the need for in situ gasification and slower reaction kinetics [18–20]. Nevertheless, research on liquid fuels in CLC remains limited. Hoteit et al. [21] investigated CLC of liquid hydrocarbons such as dodecane and heavy fuel oils in a fluidized bed reactor with Ni-based OC, reporting complete fuel conversion without carbon deposition. Similarly, Güleç et al. [22] studied higher alkanes such as n-hexadecane and n-heptane in low-temperature CLC with Cu and Mn-based OCs, achieving selective combustion and highlighting the potential of CLC for treating complex hydrocarbons. Another study by Moldenhauer et al. [23] investigated CLC of liquid fuels such as kerosene in a circulating fluidized bed reactor (CFB). Collectively, these studies confirm that CLC of relatively simple liquid fuels is feasible and highly effective.

Nevertheless, the extension of CLC to more challenging liquid feedstocks, such as the aqueous fraction of bio-oil, remains largely unexplored. Notably, most liquid-fuel CLC demonstrations to date have been conducted at comparatively high temperatures in fluidized-bed systems: Moldenhauer et al. [23] reported CLC/CLOU (Chemical Looping Oxygen Uncoupling) of kerosene with Mn- and Cu-based OCs in a 300 W circulating fluidized-bed reactor at 800–950 °C, Serrano et al. [24] demonstrated CLC of liquid fossil fuels in a 1 kWth unit using a Fe-based OC, and Rydén et al. [25] also note that suitable CLC reactor temperatures are typically in the 800–1050 °C range depending on the oxygen-carrier system. These conditions highlight the need to assess the feasibility of processing oxygenated aqueous bio-oil streams at significantly lower temperatures, where improvements in overall process efficiency may be achieved.

However, operating under such conditions introduces additional challenges that extend beyond fuel conversion and are closely linked to oxygen carrier performance and durability. A key concern is the risk of carbon deposition and carrier deactivation, particularly when using Fe-based carriers with hydrocarbons, as reported by Bao et al. [26]. Although Cu and Ni-based carriers generally exhibit higher reactivity, they may suffer from sintering or structural degradation under repeated redox cycling [27]. These issues become especially critical when dealing with oxygenated liquid fuels, whose decomposition and combustion pathways differ from those of conventional hydrocarbons. Accordingly, comprehensive reviews have emphasized the importance of developing robust OC and adapting reactor configurations to the specific characteristics of different fuel types [28].

Raw bio-oil derived from biomass pyrolysis is notoriously difficult to upgrade into high-value drop-in fuels or chemicals, largely due to its inherent instability, corrosiveness, and remarkably high-water content [4]. Within this context, the aqueous fraction of bio-oil represents an unexplored yet promising feedstock for CLC. Its high content of oxygenated compounds poses challenges for conventional thermal utilization but may align well with the reaction pathways involved in CLC, where inherent lattice oxygen can promote complete oxidation at comparatively lower temperatures. To date, however, very limited experimental evidence exists on the feasibility of applying CLC to bio-oil aqueous residues. This study fundamentally distinguishes itself from previous works by proposing a targeted integration of CLC within a biomass pyrolysis process based on an envisioned fractional condensation strategy. Feeding unrefined bio-oil directly into a combustion chamber is energy-inefficient and leads to the formation of large amounts of coke due to the thermal polymerization of heavy organic compounds [9,29]. Instead, by fractionating the bio-oil (for instance, by condensing the valuable heavy organic fractions at 120–150 °C) the remaining low-value, highly volatile aqueous fraction can be continuously fed in the vapor phase into the CLC unit. This strategic approach, which this experimental study seeks to validate at a fundamental level, mitigates operational issues and justifies the exploration of unusually low CLC operating temperatures (650–750 °C), aligning with the concept of "Low-Temperature CLC" previously demonstrated for non-condensable pyrolysis gases [30].

From a practical and scale-up perspective, a critical challenge of processing this aqueous fraction is the massive energy penalty associated with its high moisture content. However, the use of Cu-based OC provides a distinct thermodynamic advantage to overcome this barrier. Unlike other conventional transition metals, the reduction of CuO with oxygenated hydrocarbons is generally exothermic. When coupled with the strongly exothermic oxidation of Cu in the air reactor, heat is released during both half-cycles. This inherent dual exothermic nature significantly mitigates the thermal penalty of the water content, paving the way for integrated, self-heating biorefinery schemes.

In this work, a range of OCs, including Cu-, Ni-, Fe-, and Mn- based materials of both commercial origin and laboratory synthesis, were evaluated for their reactivity and carbon depositions tendency during the CLC of a model aqueous bio-oil fraction. To specifically address the poor stability and deactivation of OCs often reported in prior high-temperature CLC studies, experiments were deliberately conducted at an unusually low temperature (650 °C) to minimize thermal sintering [31,32], and align with recent advances in low-temperature CLC research [22,30,33]. Furthermore, to overcome the challenge of severe carbon deposition associated with complex liquid fuels, the tendency for carbon accumulation was systematically quantified for each active phase. The aqueous bio-oil fraction was simulated using a synthetic mixture of acetone, acetic acid, phenol, p-cresol and 2-butanone, representing the major components commonly identified in real aqueous phases derived from biomass pyrolysis bio-oil [34]. The best-performing OC was further investigated under extended redox cycling at 650 and 750 °C. Structural and textural properties were examined in the fresh, reduced, and reoxidized OC allowing assessment of redox behavior and stability under prolonged operation. The condensed products were evaluated by total organic carbon (TOC) analysis to evaluate the efficiency of CLC, while carbon deposition was determined by elemental analysis to assess combustion completeness and carbon formation. Overall, this combined approach provides valuable new insights into the performance and long-term durability of different OCs for the efficient CLC of aqueous bio-oil streams. In particular, this study demonstrates that the aqueous bio-oil fraction, traditionally regarded as a low-value waste stream, can be effectively valorized via CLC. By integrating waste utilization with inherent CO_2 capture, this approach contributes to the broader goals of decarbonization and circular economy.

2. Materials and methods

2.1. Experimental system and procedure

The scheme of the experimental system is shown in Fig. 1. Experiments were conducted in a tubular fixed-bed stainless steel reactor described in a previous works [35,36]. The reactor (length: 250 mm; inner diameter: 9 mm), was placed inside an electrically heated furnace located within the hot box of the setup. Reactor temperature was controlled by a PID controller connected to a type K thermocouple. Gas flow and pressure were regulated via a control panel, while liquid feed was introduced using an HPLC pump (Gilson 307) to ensure precise injection. Nitrogen, supplied through a mass flow controller, was employed both as carrier gas to transport the reactants into the reactor and as internal standard for quantitative gas analysis. The corresponding OC was loaded into the reactor as a fixed bed with a height of 5 cm, supported on inert glass wool. A liquid down-flow of 0.1 mL(STP)•min^{-1} was introduced continuously in the top part of the reactor, corresponding to a weight-to-feed ratio (W/m) of 10 gOC•min^{-1} reactant. All OC were first tested at 650 °C under atmospheric pressure, and each experiment was continued until the outlet gas composition reached a steady state (Experiments 1–7, see Table 1). This allowed evaluating the intrinsic reactivity and carbon deposition tendency of each material under identical operating conditions. The OC showing the most favorable performance (CuO/Al_2O_3 powder) was subsequently studied in greater detail, including additional experiments at 750 °C (Experiment 8) as well as long-term redox cycling at both 650 and 750 °C. The operating temperatures (650 and 750 °C) were selected to evaluate the 'low-temperature CLC' window. This range is strategically relevant for future integration with biomass pyrolysis units, as it maintains a suitable thermal gradient for heat transfer while preventing excessive thermal stress and sintering of the Cu-based OC. Downstream of the reactor, the effluent stream was passed through a condenser to collect condensable species, while the non-condensable gases were analyzed online using an Agilent 3000 Micro-GC enabling quantitative determination of H_2, CO, CO_2 and CH_4. Only in Experiment 9, and subsequently in the cycling tests (Experiments 10–12), the amount of CuO/Al_2O_3 powder was doubled while maintaining the same bed height by reducing the amount of inert material. This allowed extending the reduction period and

Table 1
CLC tests performed and experimental conditions.

Experiment	OC	Temperature [°C]	OC Mass [g] [(a)]	Test type
1	CuO/Al_2O_3	650	2.68	Reduction
2	Carulite	650	3.03	Reduction
3	CuO/Al_2O_3 and Carulite	650	1.42 Al_2O_3 1.42 Carulite	Reduction
4	FeO/Al_2O_3	650	2.68	Reduction
5	NiO/Al_2O_3 (powder)	650	0.91	Reduction
6	CuO/Al_2O_3 (commercial)	650	2.68	Reduction
7	CuO/Al_2O_3 (powder)	650	1.34	Reduction
8	CuO/Al_2O_3 (powder)	750	1.34	Reduction
9	CuO/Al_2O_3 (powder)	650	2.68	Reduction
10	CuO/Al_2O_3 (powder)	650	2.68	Cycles (x10)
11	CuO/Al_2O_3 (powder)	750	2.68	Cycles (x10)
12	CuO/Al_2O_3 (powder)	750	2.68	Cycles (x30)

[(a)]The mass of each OC was calculated to provide an equivalent amount of available lattice oxygen in all screening experiments, ensuring a constant oxygen-to-fuel ratio for comparative purposes.

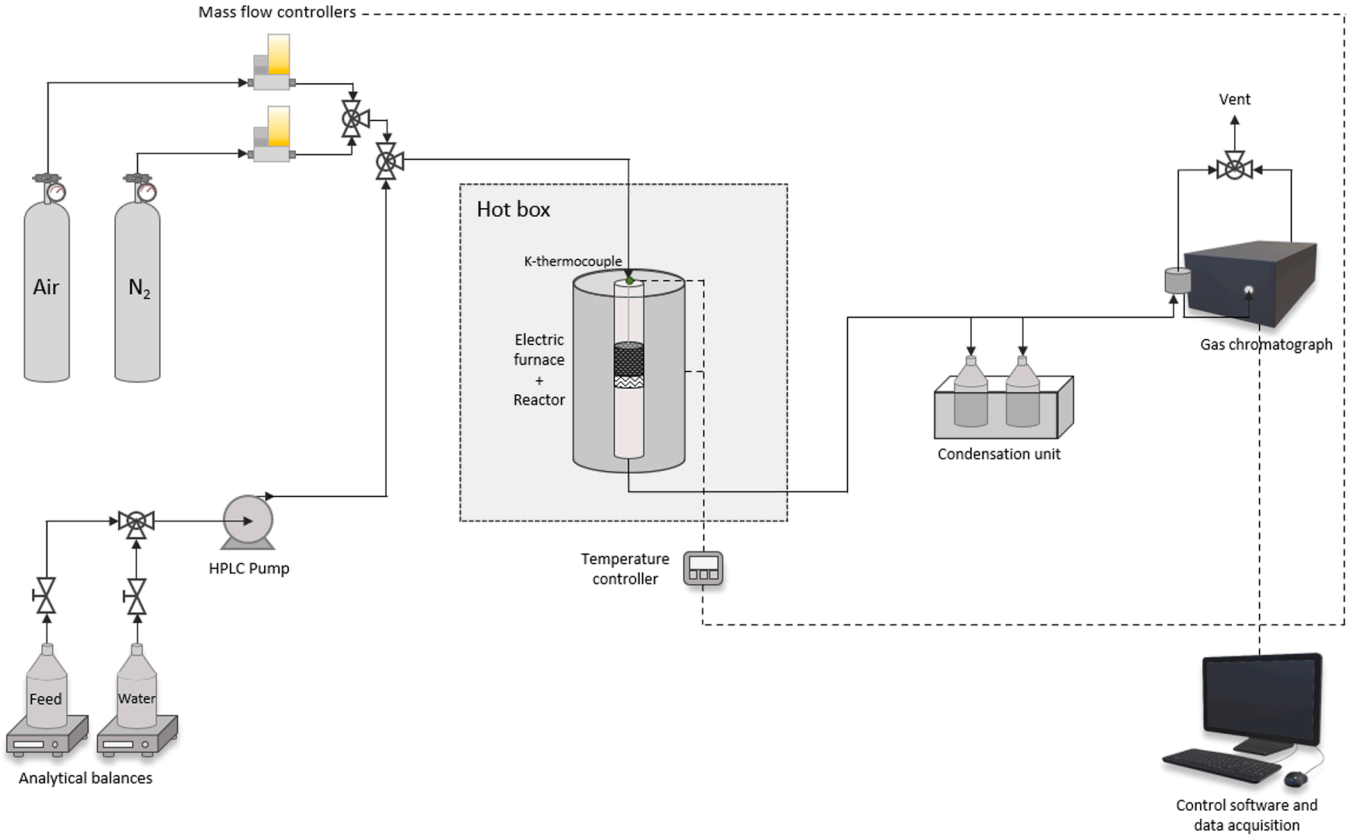

Fig. 1. Diagram of the experimental system for the CLC of liquid bio-oil phase [35,36].

improving the temporal resolution of the Micro-GC measurements, which is particularly important given the 3 min sampling interval. Redox cycling experiments consisted of 10 (Experiments 10–11) and 30 (Experiment 12) consecutive cycles carried out over a total duration of 8 h (10 cycles) and 24 h (30 cycles), corresponding to individual cycles of 48 min. Each cycle comprised four sequential steps: (i) a reduction step of 18 min, during which the complete model mixture was fed at 0.1 mL(STP)·min^{-1} together with N_2 at 30 mL(STP)·min^{-1}; (ii) a purge step of 9 min with N_2 at 100 mL·min^{-1}; (iii) a reoxidation step of 12 min carried out with air at 200 mL·min^{-1}; and (iv) a final purge of 9 min with N_2 at 100 mL·min^{-1} before initiating the next reduction step. Redox cycling was performed at both 650 and 750 °C, including single-cycle and 10-cycle experiments at each temperature, to evaluate reactivity, oxygen transfer capacity, structural stability, and resistance to carbon deposition. 30-cycle experiment was carried out at 750 ºC, since it offered the best results, as will be discussed later in results section.

2.2. Liquid fuel (aqueous phase)

The aqueous fraction of bio-oil, typically formed during storage or phase separation of pyrolysis liquids, is characterized by a very high-water content and a complex mixture of oxygenated organics including acids, ketones, and phenolics [3,37]. In the samples of the aqueous phase of bio-oil obtained in a pilot-scale biomass pyrolysis plant, Karl Fischer analysis revealed a water content of 85 wt% [34], which is consistent with previous reports that highlight the highly dilute nature of this phase [4]. Owing to its low heating value and corrosive character, this fraction is usually considered a low-value by-product. Nevertheless, its composition makes it an interesting candidate for CLC, where oxygenated species can undergo efficient oxidation at relatively low temperatures.

To simulate this aqueous phase in a reproducible manner, a synthetic model mixture was prepared based on the characterization of a real bio-oil obtained from a pilot-scale biomass pyrolysis plant described elsewhere [34]. The raw bio-oil was first decanted to separate the aqueous fraction, which was then analyzed by gas chromatography-mass spectrometry (GC-MS, Agilent Serie 7890 A) to identify the main organic constituents. Once the major compounds were identified, they were quantified by gas chromatography with flame ionization detection (GC-FID, Agilent HP-FFAP 19091F-105 capillary column). For this purpose, external calibration curves were constructed for each individual compound using high-purity standards to ensure accurate quantification of the real sample. Based on these results, five representative compounds were selected (acetone (CAS: 67–64–1), acetic acid (CAS: 64–19–7), phenol (CAS: 108–95–2), p-cresol (CAS: 106–44–5), and 2-butanone (CAS: 78–93–3)) to formulate the synthetic mixture. The final mass composition of the model mixture is summarized in Table 2. While the raw aqueous phase typically contains over 85 wt% water, the synthetic model mixture was formulated with 96.13 wt% water (Table 2). This higher water content results from selecting only the five most representative light oxygenated compounds to represent the organic fraction, omitting the heavy oligomers and hundreds of trace compounds present in real bio-oil. Furthermore, this deliberate dilution ensured a stable, single-phase liquid that prevented blockages in the micro-feeding system, allowing for a systematic, fundamental evaluation of the OCs intrinsic reactivity. These compounds cover the main functional groups typically found (ketones, acids, and phenolics) and provide a representative reactivity profile. The use of model mixtures is particularly relevant in this case because raw aqueous bio-oil is a highly complex and unstable matrix containing hundreds of compounds, many of which can interfere with systematic analysis. Furthermore, its corrosive and heterogeneous nature complicates direct use in laboratory reactors. Therefore, this preliminary study focuses on representative compounds to enable a cleaner and more controlled evaluation of reactivity under CLC conditions. This approach enables a clearer interpretation of the oxidation behavior, while avoiding the additional variability introduced by the full mixture, which remains scarcely studied in literature. Similar strategies have been employed in previous CLC studies with liquid fuels, where simplified feeds are used to systematically investigate oxidation pathways [21,22].

Table 2
Mass composition of the model aqueous phase of bio-oil.

Component	Mass weight [wt%]	CAS
Acetone	1.73	67–64–1
Acetic acid	0.31	64–19–7
Phenol	0.94	108–95–2
P-cresol	0.42	106–44–5
2-butanone	0.47	78–93–3
Water	96.13	7732–18–5

Table 3
TOC in the condensed liquid phase.

Experiment	OC	T [°C]	TOC (ppm C)	C conversion (%)	Carbon content (wt%)
1	CuO/Al_2O_3	650	3765 ± 61	80.4 ± 0.4	0.95 ± 0.40
2	Carulite	650	229 ± 1	98.8 ± 0.1	0.95 ± 0.09
3	CuO/Al_2O_3 and Carulite	650	963 ± 10	95.0 ± 0.1	BDL
4	FeO/Al_2O_3	650	792 ± 12	95.9 ± 0.1	BDL
5	NiO/Al_2O_3 (powder)	650	0	100 ± 0.0	BDL
6	CuO/Al_2O_3 (commercial)	650	1938 ± 19	89.9 ± 0.1	0.96 ± 0.05
7	CuO/Al_2O_3 (powder)	650	340 ± 67	98.2 ± 0.3	1.86 ± 0.05
8	CuO/Al_2O_3 (powder)	750	33 ± 24	99.8 ± 0.1	BDL
9	CuO/Al_2O_3 (powder)	650	0	100 ± 0.0	BDL
10	CuO/Al_2O_3 (powder)	650	0	100 ± 0.0	BDL
11	CuO/Al_2O_3 (powder)	750	0	100 ± 0.0	BDL
12	CuO/Al_2O_3 (powder)	750	0	100 ± 0.0	BDL
-	Aqueous feed (reference)	-	19239 ± 78	-	-

2.3. Preparation of oxygen carriers

Several OCs were evaluated in this study, including Cu-, Fe-, Mn- and Ni-based materials supported on Al_2O_3, as well as commercially available Cu-based formulations and a Mn-Cu mixed oxide (carulite). Alumina (CAS: 1344–28–1) was selected as support due to its high surface area, thermal stability, and mechanical resistance, which are essential properties for CLC applications [28,30].

The laboratory-prepared CuO/Al_2O_3 OC used in Experiment 1 was synthesized by incipient wetness impregnation of γ-Al_2O_3 with an aqueous solution of copper nitrate (CAS: 10031–43–3), followed by drying and calcination at 800 ºC for 5 h. The detailed preparation procedure and physicochemical properties of this material are reported in a previous work [30], where a nominal CuO loading of 20 wt% was targeted. Experiment 2 employed Carulite (CAS: 185036–38–8), a commercial Mn-Cu mixed oxide [38], which was used as received without further modification. Carulite composition and redox behavior under low-temperature CLC conditions have been previously characterized and reported in the literature [30]. Experiment 3 consisted of a physical mixture of the CuO/Al_2O_3 OC from Experiment 1 and commercial carulite in equal mass proportions, maintaining the same total oxygen

inventory as in the single-carrier experiments. Fe-based OC used in Experiment 4 was prepared following the same incipient wetness impregnation methodology as the CuO/Al_2O_3 material [30]. For the OC synthesis an iron nitrate precursor (CAS: 7782–61–8) and alumina (CAS: 1344–28–1) were employed for achieving a nominal FeO loading of 20 wt% followed by drying and calcination at 850 ºC. Ni-based OC employed in Experiment 5, consisting of coprecipitated NiO/Al_2O_3 in powder form, was prepared and characterized following the methodology described in a previous study [35].A commercial CuO/Al_2O_3 (CAS: 1317–38–0) OC was used in Experiment 6. This material, supplied by Sigma-Aldrich, was employed as received and serves as a benchmark to compare laboratory-synthesized and commercially available Cu-based formulations (13 wt% Cu). Finally, a CuO/Al_2O_3 OC in powder form was synthesized and tested in Experiments 7–11. This material was prepared following the same coprecipitation method used for the NiO/Al_2O_3, but using copper nitrate (CAS: 10031–43–3) as precursor. The synthesis procedure and baseline characterization of this powdered CuO/Al_2O_3 OC have been reported previously [35]. Owing to its superior performance in the screening experiments at 650 °C, this material was selected for temperature-effect studies and long-term redox cycling experiments.

2.4. Oxygen carrier characterization

The OCs were characterized using a combination of complementary analytical techniques in order to assess their structural, textural and chemical properties, as well as carbon formation during CLC operation.

Textural properties were determined by N_2 adsorption-desorption with an Autosorb iQ3 gas sorption analyzer from Quantachrome Instruments. The unit degassed the catalysts at 300 ∘C for 16 h and the analysis was performed at 196 °C to measure the N_2 adsorption–desorption isotherms in the range from $P/P0 = 0–1$. The surface area and pore size distribution in the adsorption branch were determined with the BET (Brunauer-Emmett-Teller) and BJH (Barrett- Joiner-Halenda) methods, respectively. X-ray diffraction (XRD) was employed to identify the crystalline phases present in the best-performing OC and to evaluate possible structural changes after redox cycling. Diffractograms were recorded using a D-Max Rigaku Ru 300 diffractometer with a rotating copper anode and a graphite monochromator emitting a CuKα radiation of $\lambda CuK\alpha = 0.15418$ nm and operating at 40 kV, 80 mA and atmospheric pressure. Data were taken over a 2θ interval from 10º to 85º at a rate of 0.03 º/s. Crystalline phase assignment was done using the JCPDS database and the crystallite sizes were calculated using the Scherrer equation. Carbonaceous deposits on the OCs after CLC experiments were quantified by ultimate analysis on a Leco CHN628 elemental analyzer equipped with NDIR infrared cells. Samples were placed in a chamber with an inert atmosphere where they were completely combusted. The CO_2 generated during combustion was quantified by infrared cells to determine the carbon composition of the sample. In addition, the organic carbon content of the condensed liquid phase collected downstream of the reactor was measured using a Total Organic Carbon Analyzer (TOC-L). TOC measurements were used to evaluate the carbon conversion of the aqueous bio-oil model compounds during the reduction step. Additionally, thermogravimetric analysis (TGA) under an oxidative atmosphere was performed to evaluate the nature and reactivity of the carbonaceous deposits. This specific characterization was conducted solely on the spent samples of the optimum OC selected to study the effect of the operating temperature. For the TGA analysis, the spent samples were first dried under a N_2 atmosphere until a constant mass was reached. Subsequently, the oxidation step was performed using a 5% O_2/N_2 gas mixture, heating the samples from 100 °C to 900 °C at a rate of 10 °C/min. Together with the gas analysis, the TOC of the liquid condensed products and the elemental analysis of the solid carrier provided the basis for evaluating the carbon distribution. Due to the inherent difficulties in achieving a strict quantitative mass closure in lab-scale setups with volatile liquid mixtures (e.g., line hold-ups and micro-condensation), these combined techniques were utilized to evaluate the relative partitioning of carbon across the gas, liquid, and solid phases. Special emphasis was placed on the elemental analysis of the solid, as it directly and accurately quantifies the carbon deposited on the oxygen carrier, which is the critical parameter governing deactivation.

3. Results

3.1. Screening of oxygen carriers

The initial evaluation of the OCs was carried out through isothermal reduction experiments at 650 °C in a fixed-bed reactor, with the aim of screening their performance during the CLC of the aqueous bio-oil model mixture. These screening tests (Experiments 1–7, Table 1) were performed under identical operating conditions. To ensure a fair and direct comparison during the screening tests, the mass of each OC loaded into the reactor (Table 1) was specifically calculated based on its theoretical oxygen transport capacity. This approach guaranteed that a constant amount of available lattice oxygen was present in the bed for all materials. Consequently, with a constant fuel feed rate, the stoichiometric ratio of available oxygen to the bio-oil fed was consistent across all screening experiments. Furthermore, to ensure a constant bed height across all experiments, the required amount of OC was mixed with an inert material (sand). This approach enables a direct comparison of the different OCs in terms of outlet gas composition, oxidation selectivity and temporal stability. In these continuous fixed-bed reduction experiments, the evolution of the product gases typically exhibits two distinct regimes as the reaction progresses. Initially, a complete combustion regime is observed, where the fully oxidized carrier provides abundant lattice oxygen to the fuel, resulting in a gas stream predominantly composed of CO_2 (and H_2O). As the experiment proceeds and the available lattice oxygen becomes depleted, the system transitions into an incomplete oxidation regime. During this stage, the OC can no longer fully oxidize the organic model compounds, leading to a steady evolution of partially oxidized products, syngas (H_2 and CO), and unreacted carbon-containing species (CH_4). To aid in the interpretation of the results, these two regimes have been visually highlighted with background colors in the subsequent figures.

Fig. 2**a** (Experiment 1, CuO/Al_2O_3) shows a rapid establishment of an outlet gas composition dominated by CO_2, with very low concentrations of CO, CH_4 and H_2. This behavior is consistent with the high oxygen transport capacity and fast redox kinetics typically reported for Cu-based carriers in CLC, which favor complete oxidation of hydrocarbons and oxygenated fuels at moderate temperatures [22,27,30,39,40]. In this experiment, an initial stage (over 3 min) dominated by CO_2 is observed, corresponding to the period in which lattice oxygen is still available and complete oxidation of the feed occurs. As the OC becomes progressively reduced, the outlet composition transitions to a stable reforming-dominated regime characterized by H_2 as the major product and minor amounts of CO and CH_4. This stationary composition reflects the establishment of oxygen-deficient conditions rather than sustained full combustion and is consistent with the well-known reduction pathway of CuO/Al_2O_3 under CLC conditions.

When carulite (Mn-Cu mineral mixed oxide) is used as OC (Experiment 2, Fig. 2**b**), the outlet gas composition also shows a predominance of CO_2, however, complete oxidation is only sustained for approximately the first 3 min of operation, after which a higher fraction of CH_4 is observed. Carulite exhibits a sustained oxidation capability, maintaining a CO_2 concentration above 80% for approximately 1 h, compared to slightly more than 20 min observed for the CuO/Al_2O_3 OC. Mixed Mn-Cu oxides have been reported as highly active materials for the oxidation of both gaseous and liquid hydrocarbons, particularly under low-temperature CLC and CLOU conditions, but their selectivity and redox stability can be sensitive to operating conditions and fuel composition [22,28,30,39]. The present results suggest that carulite is able to oxidize

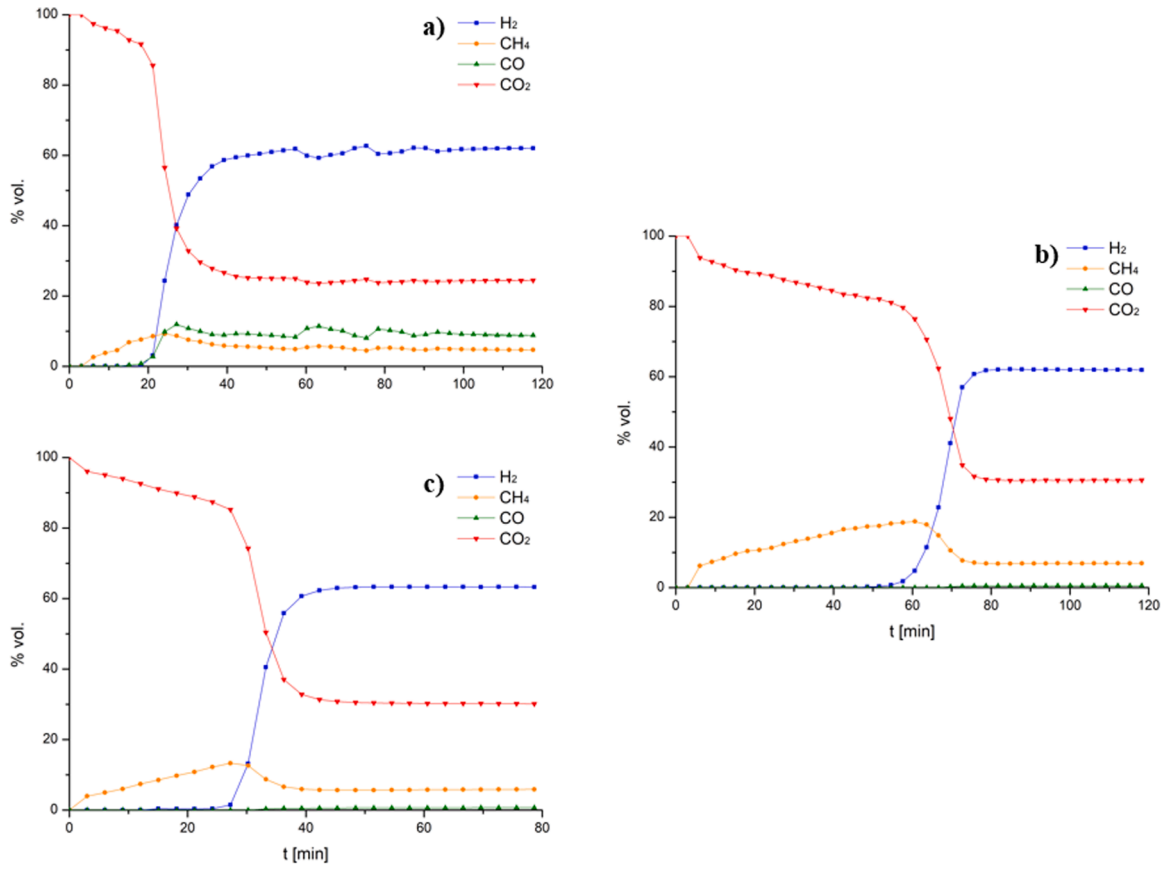

Fig. 2. Evolution of the composition of the outlet gas during OC reduction until reaching a steady state, N_2 and water free basis. a) Exp. 1; b) Exp. 2; c) Exp. 3.

the model aqueous mixture efficiently at 650 °C, but with slightly lower selectivity to fully oxidized products compared to CuO/Al_2O_3, in line with earlier observations for Mn-based carriers [22,30].

The physically mixed bed containing equal masses of CuO/Al_2O_3 and carulite (Experiment 3, Fig. 2**c**) exhibits an intermediate behavior between the two individual OC. CO_2 concentration reaches 100% only during the initial instants of the experiment, however, it remains above 80% for approximately 30 min. As previously observed for carulite alone, a higher amount of CH_4 is produced compared to the experiment using CuO/Al_2O_3 as the sole OC. In contrast, and similarly to Experiment 2, H_2 is not detected throughout the reduction period. This suggests that the two materials contribute concurrently to oxygen transfer, with the Cu-based fraction enhancing total oxidation and the Mn-based fraction promoting additional dehydrogenation and water-gas shift (WGS) pathways, as previously proposed for mixed Cu-Mn systems [22,28,30]. Although the physical mixture of CuO/Al_2O_3 and carulite did not outperform the individual materials, these findings highlight the potential value of optimizing the Cu-Mn ratio, as tuning the metal proportions could better integrate the high oxygen transport capacity of manganese with the strong ability of copper to ensure complete combustion and suppress CH_4 formation.

The Fe-based carrier (FeO/Al_2O_3) (Experiment 4, Fig. 3**a**) displays a markedly different reduction profile. The outlet gas contains significant amounts of H_2 together with noticeable CH_4 and CO from the very beginning of the experiment. Complete oxidation to CO_2 is only observed during the initial instants, after which the CO_2 concentration drops abruptly and stabilizes at around 40%. This behavior is markedly different from that observed with Carulite (Experiment 2) and other Cu- and Mn-Cu-based materials, which exhibit substantially higher and more sustained CO_2 fractions. This behavior is consistent with the lower oxygen transport capacity and slower kinetics of Fe_2O_3-based carriers in this temperature range, which often lead to incomplete combustion or partial oxidation, especially when dealing with complex or highly oxygenated fuels [28,41,42]. The relatively short duration of the experiment until steady state is reached further reflects the limited reactive capacity of the Fe-based OC under the present conditions, however, its low cost and benign nature justify further research to enhance its reactivity. Strategies such as doping with transition metals (Cu or Ni) to improve oxygen transfer kinetics, or using alternative supports like ZrO_2 or TiO_2 to prevent the formation of thermally stable but less reactive iron aluminate spinels could increase its applicability in low-temperature processes. Additionally, increasing the active phase loading may offset its lower oxygen transport capacity compared to Cu-based carriers.

In contrast, the Ni-based OC (Experiment 5, Fig. 3**b**) shows a reduction profile dominated by a high and persistent H_2 concentration, accompanied by moderate CO_2 formation and negligible CO and CH_4 once the initial transient has passed. This behavior indicates that, under the present operating conditions (650 °C and a highly oxygenated aqueous feed), NiO/Al_2O_3 rapidly reaches oxygen-deficient states, and the reduced Ni phase catalyzes steam reforming and WGS reactions rather than sustaining complete combustion [43]. Similar transitions from combustion to reforming have been widely reported for Ni-based OCs when the OC to fuel ratio is low or when the solid becomes significantly reduced [39,44,45]. However, it is important to note that NiO is generally considered one of the most reactive OCs for CLC at higher temperatures (800–950 °C), where its fast redox kinetics enable full conversion of a wide range of gaseous and liquid fuels [28,39,46]. The high H_2 concentrations observed do not indicate an inherent inadequacy of Ni-based OC for CLC, but rather reflect the specific operating conditions of the present fixed-bed experiments, where at 650 °C and under oxygen-lean conditions NiO is rapidly reduced and predominantly behaves as a reforming catalyst instead of as an effective OC [43]. This pronounced tendency of NiO/Al_2O_3 toward steam reforming

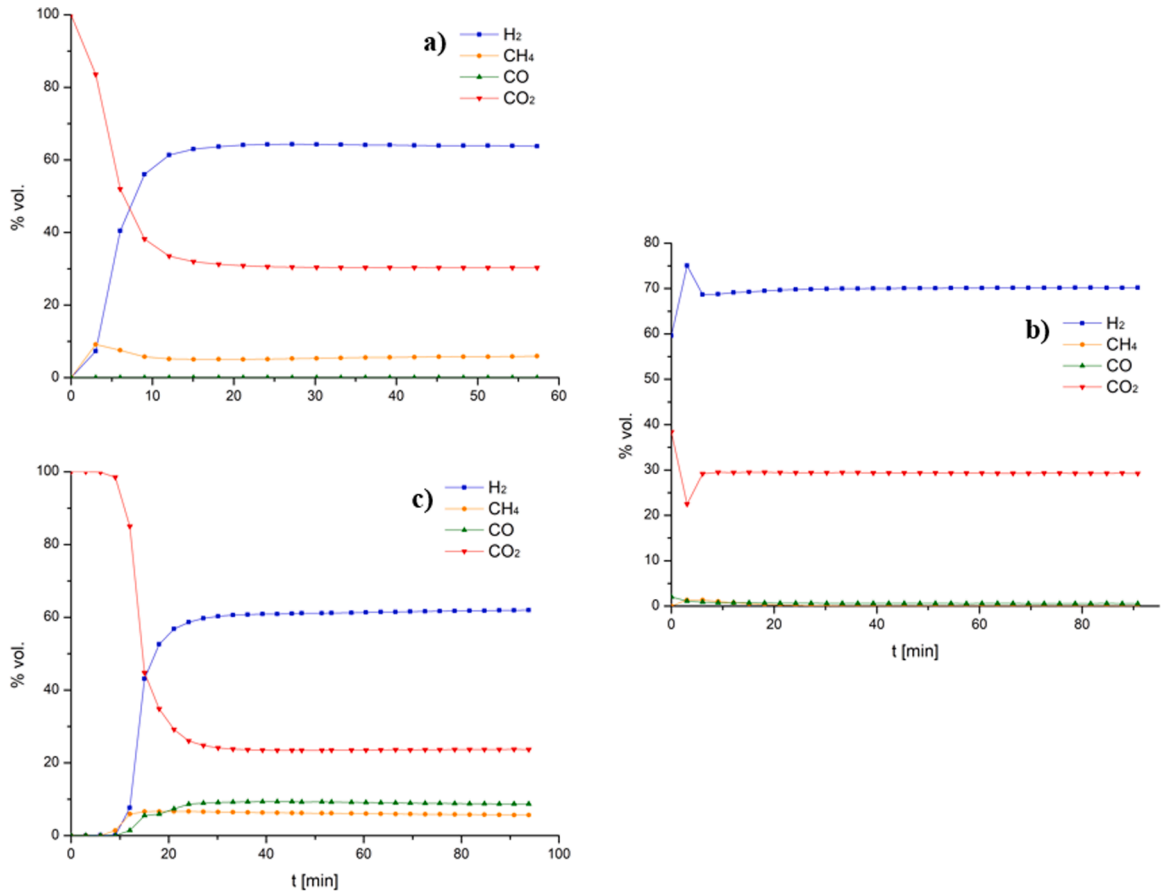

Fig. 3. Evolution of the composition of the outlet gas during OC reduction until reaching a steady state, N_2 and water free basis. a) Exp. 4; b) Exp. 5; c) Exp. 6.

and WGS, promoted by the high water content of the bio-oil aqueous phase (96.13 wt%), further suggests that this material is highly suitable for reforming. In this context, the aqueous fraction from pyrolysis, traditionally regarded as a low-value by-product, could be valorized not only for energy generation via CLC but also as a renewable feedstock for syngas or hydrogen production using Ni-based carriers [47].

The commercial CuO/Al_2O_3 OC (Experiment 6, Fig. 3**c**) shows an outlet gas composition qualitatively similar to that of the laboratory-prepared CuO/Al_2O_3 (Experiment 1), with CO_2 as the main product and low concentrations of CO, CH_4 and H_2 after the initial transient. Complete oxidation to CO_2 is maintained for approximately 9 min (higher than in Experiment 1), after which minor amounts of H_2, CH_4 and CO begin to appear. The slightly shorter time required to reach steady state, despite using the same mass of OC and operating conditions, suggests a marginally higher effective reactivity of the commercial material, which may be related to differences in CuO dispersion, porosity or mechanical properties, as previously reported for industrial CuO/Al_2O_3 formulations in pilot-scale CLC units [28,48].

The last OC studied in the screening was the Cu-based CuO/ Al_2O_3 powder (Experiment 7, Fig. 4**a**). This OC is able to oxidize the aqueous phase for approximately 12 min before CH_4 begins to appear, representing the longest period of sustained oxidation among all OCs tested under identical conditions. Only after an extended combustion phase does the gas composition shift toward a reforming-dominated regime, reflected by increasing H_2 levels and a gradual decline in CO_2. This behavior highlights the superior oxidative capacity and slower oxygen depletion of the CuO/ Al_2O_3 powder at 650 °C.

Overall, the comparison of Experiments 1–7 shows that all Cu-containing carriers (laboratory-prepared CuO/ Al_2O_3, commercial CuO/ Al_2O_3 and CuO/ Al_2O_3 powder) and the Mn-Cu mixed oxide (carulite) are able to combust the model aqueous mixture with very high selectivity to CO_2 under the tested conditions. Cu-based OC are widely reported as promising candidates for chemical looping applications due to their high oxygen transport capacity, fast redox kinetics and relatively low carbon deposition compared to Fe-based materials [26,28,49]. Their favorable reactivity in the moderate temperature range (500–700 °C) also aligns with the operating conditions employed in this work and helps mitigate sintering effects typically observed at higher temperatures [14,28]. Whereas the Fe-based carrier exhibits limited reactivity and the Ni-based carrier promotes extensive H_2 formation rather than complete oxidation. These trends are fully consistent with the general ranking of CLC OCs reported in the literature. Cu-based materials are typically highlighted for their high oxygen transport capacity and fast redox kinetics. Mn-based carriers for their robustness and intermediate reactivity. Fe-based carriers for their low cost but lower activity, while Ni-based carriers for their high activity but stronger tendency toward reforming and carbon-related phenomena [28,39,50]. This supports the selection of CuO/Al_2O_3 powder as the most suitable OC for the subsequent long-term redox cycling experiments.

To systematically summarize the observed experimental trends, the performance of the evaluated OCs at 650 °C is strongly dictated by the competition between their intrinsic redox thermodynamics and their catalytic properties. A clear regularity can be established: carriers such as Cu- and Mn-based materials exhibit superior performance for complete combustion due to their highly favorable reduction kinetics at moderate temperatures and their high lattice oxygen mobility, including potential CLOU capabilities [51]. This facilitates the direct and complete oxidation of the complex oxygenated molecules. Conversely, Ni- and Fe-based materials demonstrated a rapid transition toward an incomplete oxidation regime. Nickel, in particular, is a well-known, highly active catalyst for C-C bond cleavage and steam reforming [52,47]. Given the highly aqueous nature of the fuel mixture (96 wt% water), the

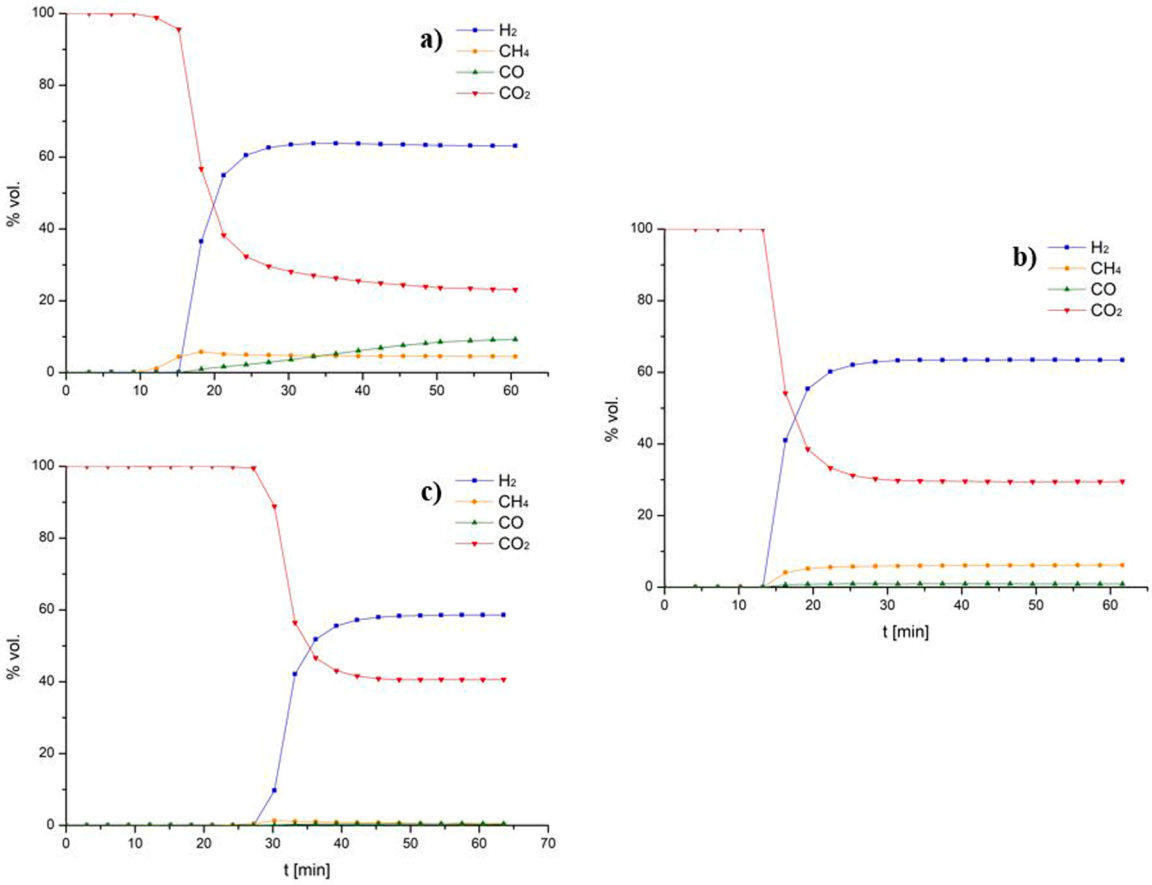

Fig. 4. Evolution of the composition of the outlet gas during OC reduction until reaching a steady state, N_2 and water free basis. a) Exp. 7; b) Exp. 8; c) Exp. 9.

steam reforming reactions over the reduced Ni (and Fe) species kinetically outcompete the direct solid-gas oxidation reactions. Consequently, this leads to the substantial formation of syngas (H_2 and CO) rather than CO_2. This screening clearly establishes that, for the specific valorization of highly diluted aqueous bio-oil at low temperatures via CLC, carriers with high oxidation potential and low reforming catalytic activity (like Cu) are essential, whereas Ni-based materials direct the process towards Chemical Looping Reforming (CLR) [53,54].

3.2. *Effect of the temperature on the reduction behavior of the selected CuO/Al_2O_3 powder*

Following the screening study presented previously, the CuO/Al_2O_3 powder was identified as the most effective oxygen carrier for the oxidation of the aqueous bio-oil model mixture under identical operating conditions, as it exhibited the longest period of complete oxidation at 650 °C and the slowest transition toward oxygen-deficient regimes. Consequently, this material was selected to evaluate the influence of temperature on its reduction behavior. A direct comparison between Experiment 7 (Figs. 4**a**) and 8 (Fig. 4**b**) allows the effect of increasing the operating temperature from 650 to 750 °C to be assessed while keeping the OC mass and all other experimental conditions constant. At 650 °C the CuO/Al_2O_3 powder displays an extended period of complete combustion, followed by a gradual shift toward a reforming-dominated regime, as discussed in the previous section. When the same OC is operated at 750 °C, complete conversion is observed in the first part of the experiment. The behavior in the oxidation is slightly higher than 650 °C. It can be seen that at around 12 min it still oxidizes completely, whereas in experiment 7 a drop in the percentage of CO_2 can already be observed. H_2 and CH_4 behave in the same way as at 650 °C, while at 750 °C CO formation is lower, indicating better oxidation of the fuel to CO_2. This behavior demonstrates that the increase in temperature enhances both oxygen transfer kinetics and the effective oxidizing capacity of the CuO/Al_2O_3 powder, allowing fully oxidizing conditions to be sustained over longer periods. These results confirm the very high reactivity of the CuO/Al_2O_3 powder at elevated temperatures and are consistent with earlier studies reporting rapid redox kinetics and excellent combustion performance for Cu-based oxygen carriers operating in the 700–800 °C range [28,30,55,56,57].

3.3. *Effect of the oxygen carrier loading at constant bed height*

To further investigate the influence of oxygen carrier inventory on the reduction behaviour of the selected CuO/Al_2O_3 powder, Experiment 9 was performed at 650 °C using twice the OC mass (2.68 g) while maintaining the same bed height by reducing the amount of inert material (Fig. 4**c**). This configuration was adopted primarily to extend the reduction period, allowing a better temporal resolution of the outlet gas composition given the discrete sampling interval of the Micro-GC. Compared to Experiment 7 (Fig. 4**a**), carried out at the same temperature but with half the OC mass, the overall reduction behavior remains qualitatively similar. The outlet gas composition is dominated by CO_2 during the initial stage, followed by a gradual transition toward a reforming-dominated regime as lattice oxygen becomes depleted. However, increasing the OC mass significantly prolongs the period of complete oxidation. In Experiment 9, full conversion to CO_2 is sustained for approximately 30 min, which is markedly longer than in Experiment 7. Once steady-state conditions are reached, the outlet gas composition exhibits negligible amounts of CH_4 and CO, while H_2 becomes the dominant product, following a similar trend to that observed in

Experiments 7 and 8. This indicates that doubling the OC inventory primarily increases the available lattice oxygen and delays its depletion, without fundamentally altering the reaction pathways governing the transition from combustion to reforming. Overall, results demonstrate that, at 650 °C, the CuO/Al_2O_3 powder can achieve a combustion performance comparable to that observed at higher temperature, provided that sufficient oxygen carrier inventory is available. Given the very similar reduction behavior observed at 650 and 750 °C for this material (Experiments 7 and 8), a comparable extension of the complete oxidation period would also be expected at 750 °C when increasing the OC mass. This finding justifies the selection of the higher OC mass configuration for the subsequent redox cycling experiments, ensuring extended reduction periods compatible with the temporal resolution of the analytical system.

3.4. CLC performance over multiple cycles

The long-term redox stability of the CuO/Al_2O_3 powder was evaluated at 650 and 750 °C over 10 consecutive cycles with a total duration of 8 h, following the procedure and conditions described in 2.1. Experimental system and procedure. Throughout these cycles, gas analysis confirmed that only CO_2 was produced during reductions, with no detection of unreacted CH_4, CO, or any other secondary by-products. Fig. 5 and Fig. 6 show the evolution of O_2 and CO_2 concentrations during the reoxidation stages at 650 and 750 °C, respectively. At both temperatures, the OC exhibits highly stable and reproducible redox behavior. The O_2 profiles during the air steps remain essentially unchanged throughout the cycling experiments, indicating complete regeneration of the reduced copper phase and the absence of progressive deactivation. This confirms the regenerability of the CuO/Al_2O_3 powder under cyclic CLC operation, in agreement with previous studies on Cu-based OCs [22,28,30,39,50]. A marked temperature effect is observed with respect to carbon-related phenomena. At 650 °C (Fig. 5), distinct CO_2 peaks appear systematically during each reoxidation step. These peaks are attributed to the oxidation of carbon species deposited on the OC during the preceding reduction stage, indicating that limited carbon formation occurs at this temperature. In contrast, at 750 °C (Fig. 6) the CO_2 signals during reoxidation are strongly reduced or nearly absent, demonstrating that carbon deposition is largely suppressed at a higher temperature. This behavior is consistent with the enhanced oxygen mobility and faster surface reaction kinetics of Cu-based carriers at elevated temperatures, which favors complete oxidation of the fuel during reduction and hinder carbon accumulation [28,39]. In both cases, gas-phase oxidation during the reoxidation steps is complete, and the OC maintains its full activity over repeated cycles. In addition, the CO_2 peak concentration during the reduction stage increases from ~9 vol% at 650 °C to ~12 vol% at 750 °C. This difference is consistent with coke formation at 650 °C; at this temperature, a fraction of the fuel carbon undergoes surface-catalyzed reactions, generating solid carbonaceous deposits on the OC rather than being immediately oxidized to CO_2. The subsequent CO_2 peaks observed during reoxidation at 650 °C support this interpretation, as they indicate oxidation of the deposited carbon. At 750 °C, the strongly reduced/absent CO_2 signal during reoxidation suggests that such carbon deposition is largely suppressed, resulting in higher direct conversion of fuel carbon to CO_2 during reduction [30,58,59]. Overall, these results demonstrate that the CuO/Al_2O_3 powder maintains its activity over repeated cycles and demonstrates robust carbon management. Given that operation at 750 °C promoted higher in-situ conversion of fuel carbon to CO_2 and successfully minimized carbon deposition, an extended stability test was conducted at this optimal temperature to further validate its industrial potential.

Fig. 7 displays the OC performance over a 24-hour (30 cycles) continuous cyclic operation at 750 °C. As observed, the gas concentration profiles for both the reduction and oxidation steps remain highly stable from the first to the final cycle. The steady and reproducible O_2 consumption during the consecutive air steps indicates that the oxygen transfer capacity of the CuO/Al_2O_3 powder carrier is preserved throughout this period. Notably, a minor CO_2 peak is consistently detected during the reoxidation steps. This small peak, which was already beginning to be discernible during the final cycles of the shorter 10-cycle test (Fig. 6), remains constant in magnitude across the extended 30 cycles. This indicates that while a slight carbon deposition still occurs at 750 °C, it reaches a steady state and does not progressively accumulate or interfere with the carrier overall performance. This stable cyclic behavior suggests that the material resists immediate and severe

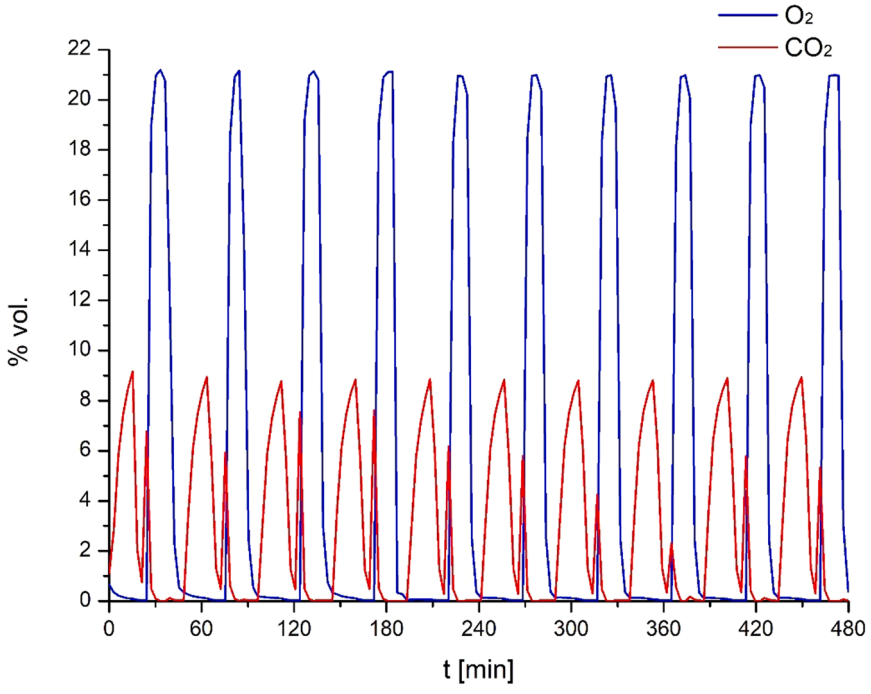

Fig. 5. CLC redox cycles with CuO/Al_2O_3 powder at 650 °C.

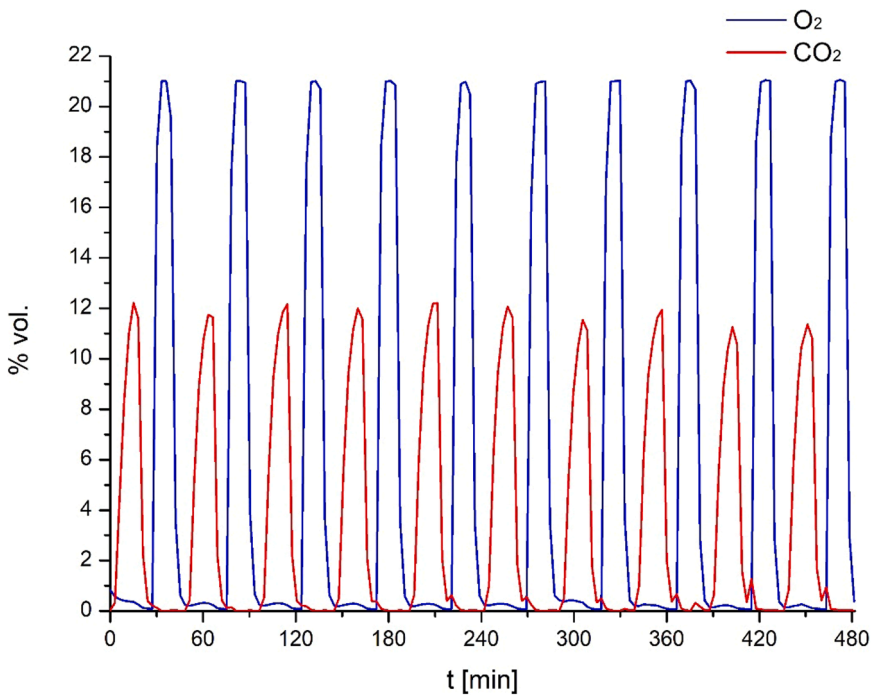

Fig. 6. CLC redox cycles with CuO/Al_2O_3 powder at 750 °C.

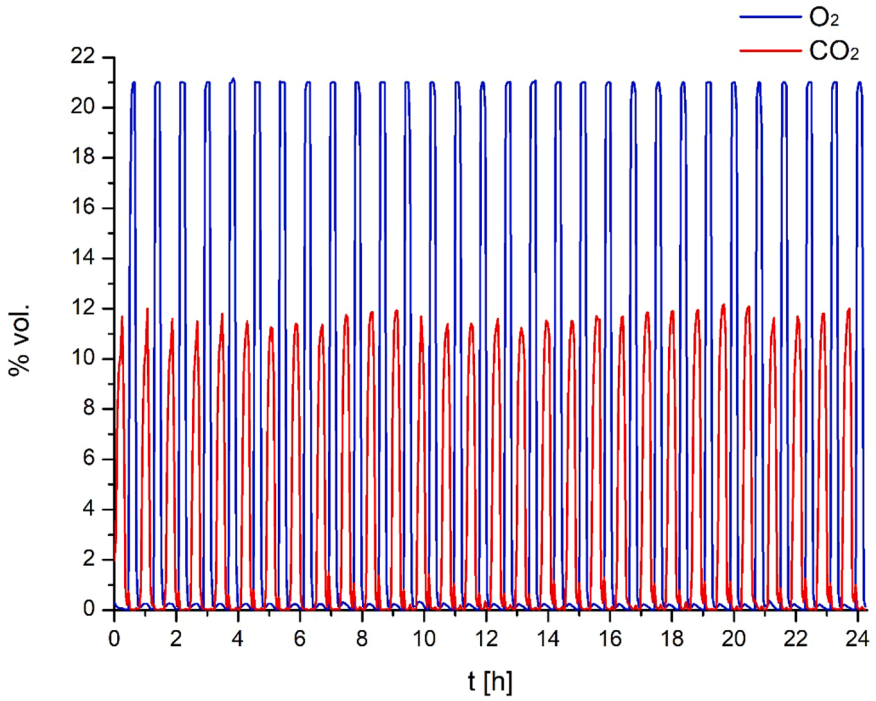

Fig. 7. CLC redox cycles with CuO/Al_2O_3 powder at 750 °C (30 cycles).

deactivation mechanisms typical of copper-based materials, such as rapid active phase sintering or structural collapse. Furthermore, the constant CO_2 production during the reduction phases verifies that the solid-gas reaction kinetics do not deteriorate over this continuous exposure. However, while these 24-hour results successfully validate the cycling stability and carbon management of the carrier at an intermediate scale, further pilot-scale studies of significantly longer duration will be required to definitively confirm the ultimate lifespan and long-term physicochemical stability of the material under industrial CLC conditions.

3.5. Carbon balance and OC stability

The extent of carbon conversion during CLC of the aqueous bio-oil was evaluated through TOC analysis of the condensed liquid phase and elemental carbon analysis of the used OCs. The corresponding results are summarized in Table 2. Carbon conversion was calculated according to (Eq. 1), based on the TOC measured in the condensed liquid

phase.

$$C\ conversion\ (\%) = \frac{TOC_{aq.\ \ feed} - TOC_i}{TOC_{aq.\ \ feed}} \bullet 100 \quad (1)$$

Where:

- $TOC_{aq.feed}$: ppm of C in the bio-oil aqueous phase (liquid feedstock).
- TOC_i: ppm of C in the obtained condensed liquid of *i* experiment.
- *i*: experiments 1–11 performed.

All experiments show a substantial reduction in the organic carbon content of the condensed liquid compared to the aqueous feed, confirming effective conversion of oxygenated compounds during the reduction step. Such a strong decrease in liquid-phase organic carbon is characteristic of CLC systems, where oxygenated fuels are readily oxidized by lattice oxygen even at moderate temperatures [28]. Nevertheless, marked differences among OCs are observed, expressed in terms of carbon conversion, this corresponds to values ranging from approximately 80% up to complete conversion, depending on the OC and operating conditions. It is important to note that the reduction experiments were not all conducted for the same total duration, as they were designed as screening tests and were terminated once a stable gas outlet composition was reached. As a consequence, the absolute TOC values of the condensed liquids are influenced not only by OC reactivity but also by the effective reduction time. This limitation must be considered when comparing experiments with different durations. Despite this constraint, direct comparisons can be made between experiments performed for identical reduction times. In particular, Experiments 1 and 2 were conducted for the same duration, allowing a meaningful comparison between CuO/Al_2O_3 and carulite, which clearly highlights the superior carbon conversion achieved by the Mn-Cu mixed oxide under identical conditions. Likewise, Experiments 7, 8 and 9, all performed with the CuO/Al_2O_3 powder and identical reduction times, can be directly compared without ambiguity.

The laboratory-prepared CuO/Al_2O_3 carrier (Experiment 1) achieves a carbon conversion of 80.4%, while the commercial CuO/Al_2O_3 formulation (Experiment 6) reaches 89.9% conversion, indicating high but incomplete oxidation under the selected conditions. Similar behavior has been reported for Cu-based OCs when oxygen availability becomes locally limited during reduction [30,39,51]. Carulite (Experiment 2) exhibits a much higher carbon conversion of 98.8%, pointing to a higher degree of carbon oxidation, consistent with its CO_2-rich outlet gas composition and the good redox stability reported for Mn-Cu mixed oxides [28,39]. The mixed-bed configuration (CuO/Al_2O_3 and Carulite) results in a carbon conversion of 95.0%, suggesting that combining OCs with different redox properties does not lead to a synergistic improvement over the best-performing single material. Fe-based carrier (Experiment 4) exhibits lower carbon conversion, reflecting its lower intrinsic reactivity toward complete oxidation of oxygenated compounds at the tested temperature, a behavior commonly reported for Fe-based OCs, which typically require higher temperatures or longer contact times to achieve full conversion [39,60]. By contrast, Ni-based carrier (Experiment 5) showed complete carbon conversion, which reflects extensive conversion of liquid-phase carbon but, as discussed previously, is associated with reforming-dominated behavior rather than complete combustion. The CuO/Al_2O_3 powder displayed the highest carbon conversion among all Cu-based materials, particularly at 750 °C (Experiment 8), where 99.8% conversion was achieved, demonstrating its superior oxidative performance. Moreover, during long-term redox cycling at both 650 and 750 °C (Experiments 10 and 11), carbon conversion remained complete, indicating stable and reproducible carbon conversion over extended operation.

Elemental carbon analysis of the spent OC (Table 2) provides complementary insights into net carbon deposition. For most OCs, net carbon deposition remained over 0 wt%, confirming a limited tendency toward solid carbon formation. The highest carbon content is observed for the CuO/Al_2O_3 powder tested at 650 °C (1.86 wt%), which is consistent with the gradual depletion of lattice oxygen at lower temperature. In contrast, carbon deposition is strongly suppressed at 750 °C and after cyclic operation, where no carbon was detected on the spent samples. In addition, analyses of the OC after the redox cycling experiments (Experiments 10 and 11) revealed negligible residual carbon, as these samples were collected after reoxidation. This clearly demonstrates that the reoxidation steps at both temperatures effectively eliminate the carbon deposits formed during reduction. Overall, the combined TOC and elemental carbon analyses confirmed that Cu-based OCs, and particularly CuO/Al_2O_3 powder, enabled efficient conversion of the aqueous bio-oil fraction with minimal residual carbon in both the liquid and solid phases, especially at elevated temperature and under cyclic operation, fully consistent with trends reported in the CLC literature [28,39,51].

Additionally, to confirm the higher carbon deposition observed in the reduction of the CuO/Al_2O_3 powder at 650 °C (Experiment 7) compared to the reduced at 750 °C (Experiment 8), TGA analyses were carried out (Fig. 7). For these spent CuO/Al_2O_3 samples, the weight gain results from the rapid reoxidation of Cu to CuO, which occurs in the 250–450 °C range [28,61]. This weight gain directly overlaps with the weight loss associated with the combustion of carbonaceous deposits. As shown in Fig. 7, the sample reduced at 750 °C (Experiment 8) exhibits a weight gain curve characteristic of pure metal reoxidation, confirming the absence of significant carbon deposition. Conversely, the profile of the sample reduced at 650 °C (Experiment 7) exhibits a pronounced decrease. This lower net weight gain is caused by the simultaneous weight loss from the combustion of deposited carbon. The deviation between the two curves occurs exclusively in the 300–500 °C range, which corresponds directly to the oxidation of soft carbonaceous depositions [62]. Notably, at temperatures above 550 °C, a slight weight loss is observed in the curves. This high-temperature decay indicates the combustion of highly ordered graphitic coke, which typically oxidizes at temperatures exceeding 550–600 °C [63]. In summary, these results provide direct evidence that carbon deposition is significantly promoted at 650 °C, while operating at 750 °C effectively reduces this phenomenon.

3.6. Characterization of the selected oxygen carrier

To gain a deeper understanding of the redox behavior and stability of the most promising OC, the CuO/Al_2O_3 powder OC was subjected to textural and structural characterization. This study focused on identifying the changes undergone after operation. The fresh OC was analyzed and compared with samples spent after tests at 650 and 750 ºC both after a single cycle and after multiple redox cycles in order to assess the impact of operating temperature and time on the physicochemical properties.

3.6.1. Textural properties

The specific surface area (S_{BET}), average pore diameter (d_p), pore volume (V_P), and pore size distribution (PSD) was evaluated by N_2 adsorption-desorption. The evolution of these parameters is a critical indicator of the thermal stability and resistance to sintering of the OC. Fig. 7**a** displays the N_2 adsorption-desorption isotherms and Fig. 7**b** the BJH PSD of all the samples, while Table 4 summarizes the textural properties.

The utilization of the Cu/Al_2O_3 powder OC during the consecutive redox cycles significantly modified its textural properties, as reflected in the N_2 adsorption-desorption isotherms and PSD. All samples exhibited a characteristic Type IV isotherm with an H2b-type hysteresis loop, which is typical of mesoporous solids with a complex structure with different shaped pores [65]. A comparative analysis reveals progressive structural modifications governed by both the operating temperature and the number of redox cycles. Compared to the fresh OC, performing 1 cycle at

Table 4
Textural and structural parameters of studied OC.

Experiment	S_{BET} [m^2/g]	V_P [cm^3/g]	d_P [nm]	D_{CuO} [nm]	$D_{CuAl2O4}$ [nm]
Fresh OC [64]	157	0.32	7.3	17	-
7	108	0.32	12.8	17	8
8	128	0.33	11.2	14	10
10	77	0.30	15.1	21	8
11	42	0.23	18.4	24	30
12	20	0.17	32.0	29	34

650 °C and 750 °C resulted in a reduction of the total N_2 uptake and hysteresis area, indicating an initial loss of surface area, decreasing to 108 and 128 m^2/g, respectively. This initial degradation is primarily attributed to the thermal sintering of both the Cu phase and the alumina support. Furthermore, the more pronounced loss of porosity observed at 750 °C is closely associated with an enhanced solid-state reaction between the metal oxide and the support. As reported in previous studies [64,66], higher temperatures thermodynamically favor the incorporation of Cu species into the alumina lattice to form the $CuAl_2O_4$ spinel, a process that inherently reduces the specific surface area of the material. Interestingly, during this initial stage, the total pore volume remained unchanged while the average pore diameter widened from 7.3 nm to 12.8 nm at 750 °C. This phenomenon is clearly evidenced by the PSD profiles. While the fresh OC exhibited a narrow distribution of mesopores concentrated in the 2–15 nm range, the operation after 1 cycle shifted the predominant pores towards larger sizes, pointing the coalescence of smaller mesopores into larger ones. This structural degradation is further exacerbated by the cyclic nature of the CLC process. Extending the operation to 10 redox cycles led to a more pronounced collapse of the mesoporous structure and $CuAl_2O_4$ formation. The cumulative structural stress induced by the repeated changes during the phase transformations between CuO and Cu, combined with the higher thermal severity at 750 °C, results in the most significant densification. Consequently, the sample operated for 10 cycles at 750 °C suffered a severe drop in surface area (42 m^2/g) and pore volume (0.23 cm^3/g), accompanied by a pore enlargement up to 18.4 nm. The PSD profile corroborates this structural degradation, displaying a severely flattened curve with its maximum shifted toward the 20–30 nm range. Nevertheless, despite the progressive loss of porosity, the material retained sufficient mesoporosity to ensure adequate reactivity during the CLC process, as seen in previous sections. In order to ensure the stability of the OC, 30 cycles have been carried out at 750 °C (Experiment 12). The results from Table 4 exhibit a clear decay of the S_{BET} value as well as the V_P to 20 m^2/g and 0.17 cm^3/g, respectively, due to a higher sintering phenomenon and carbon deposition, which may partially block the pores. The higher sintering phenomenon is confirmed by the increase in the D_{CuO} and $D_{CuAl2O4}$ values.

3.6.2. Structural characterization and evolution

In order to determine the changes of the Cu phase during the experiments, XRD analyses were performed. Fig. 7 displays the comparative diffractograms of the fresh, spent in 1 cycle, and spent in multiple cycles OC at 650 and 750 ºC, and Table 4 shows the CuO or $CuAl_2O_4$ average crystallite size calculated using the Scherrer equation. To ensure a proper assessment of the phase recovery and structural integrity, all spent samples were subjected to reoxidation before XRD.

The diffractogram of the fresh OC shows copper oxide (CuO) as the only detectable crystalline phase, evidenced by the characteristic diffraction peaks located at 2θ = 32.1º, 35.5°, 38.7°, 48.7°, 53.5°, 58.3°, 61.5°, 66.2°, and 68.0° (JCPDS 01–072–0629). The absence of peaks corresponding to aluminum species suggests that this support is in an amorphous state or acts as a highly dispersed matrix at this initial stage. The CuO average crystallite size in the fresh OC, calculated at 2θ = 35.5º, is 17 nm.

After being subjected to one redox cycle at 650 ºC, a clear increase in the crystallinity of the OC is observed, reflected in the higher intensity and sharpness of the peaks. Furthermore, the copper aluminate spinel phase ($CuAl_2O_4$) clearly emerges, identified by its characteristic reflections at 2θ = 31.3°, 36.8°, 44.8°, 55.6°, 59.3°, and 65.2° (JCPDS 01–073–1958). This indicates that the reduction-oxidation process thermodynamically promotes the solid-state reaction between CuO and the alumina support, forming $CuAl_2O_4$. The crystallite size of CuO did not increase compared to the fresh OC, and the $CuAl_2O_4$ phase showed a crystallite size of 8.0 nm. When evaluating the OC after 1 cycle at 750 ºC, a similar behavior regarding spinel formation is observed; however, in this case, the presence of metallic copper (Cu) (JCPDS 01–085–1326) is detected, as well as cuprous oxide (Cu_2O) (JCPDS 03–0898). The appearance of these reduced phases is attributable to an incomplete oxidation of the OC. The detection of metallic Cu and Cu_2O was exclusively observed in the sample after 1 cycle at 750 ºC. Furthermore, as shown in Fig. 8, the diffraction intensities for these phases are minimal, indicating that they represent only minor remnants of the reduced species that were not fully converted back to CuO. This localized incomplete oxidation is likely attributable to the initial sintering and grain growth at 750 ºC, which may slightly hinder oxygen diffusion to the innermost parts of the particles within the reoxidation timeframe. Nevertheless, these traces are negligible and do not affect the functional regenerability of the OC, as evidenced by the stable performance and complete carbon conversion maintained in the subsequent redox cycles. Compared to the OC tested for 1 cycle at 650 ºC, the crystallite size of CuO was reduced to 14 nm, possibly because of the incomplete reoxidation, while the copper spinel crystallite size increased to 10 nm. This trend can be attributed to the higher temperature of the process.

To understand the long-term structural evolution, the samples were analyzed after 10 consecutive cycles. At 650 ºC, the main phases (CuO and $CuAl_2O_4$) remain stable compared to the first cycle, but a further increase in crystallinity is evident with more defined peaks. The CuO phase increased its crystallite size up to 21 nm, while the $CuAl_2O_4$ maintained its size in comparison with the first cycle. This sintering phenomenon is common during repetitive redox cycles, as the continuous phase transitions and process temperature favor atomic mobility, promoting grain growth and thermal sintering of the crystallites [32]. On the other hand, after 10 cycles at 750 ºC, the structural transformation is more evident. A greater increase in crystallinity is observed, and the $CuAl_2O_4$ spinel phase becomes predominant compared to CuO. The crystallite sizes of the $CuAl_2O_4$ and CuO phases achieved values of 30 and 24 nm, respectively. Prolonged exposure at 750 ºC provides the activation energy and time necessary for the migration of Cu into the alumina crystal lattice, decreasing the S_{BET} [66].

It is worth noting the appearance of diffraction peaks at 2θ = 21.0°, 26.6°, 39.5°, 46.0°, and 50.0° in some of the tested OC, which are characteristic of the crystalline SiO_2 phase (JCPDS 01–085–0335). These peaks do not derive from the intrinsic structure of the OC but are a direct consequence of cross-contamination with the silica sand used as an inert material in the fixed-bed during the experiments.

Finally, structural stability was evaluated after a long-term test of 30 cycles at 750 °C. The XRD pattern of this sample shows a profile remarkably similar to the one observed after 10 cycles, indicating that the structural transformation of the OC reaches a steady state. The predominant phase remains the copper aluminate spinel ($CuAl_2O_4$) and CuO. The crystallite sizes for CuO and $CuAl_2O_4$ after 30 cycles were 29 and 34 nm (Table 4), respectively, showing an increase compared to the 10-cycle sample (24 for CuO and 30 for $CuAl_2O_4$). This indicates a higher sintering phenomenon during the cycles, as mentioned above.

3.6.3. Properties-performance correlation analysis

The experimental results revealed a clear correlation between the OC's textural and structural evolution and its performance. Observations from the first redox cycle indicate that reactivity is primarily governed by temperature-dependent kinetics rather than by the initial availability

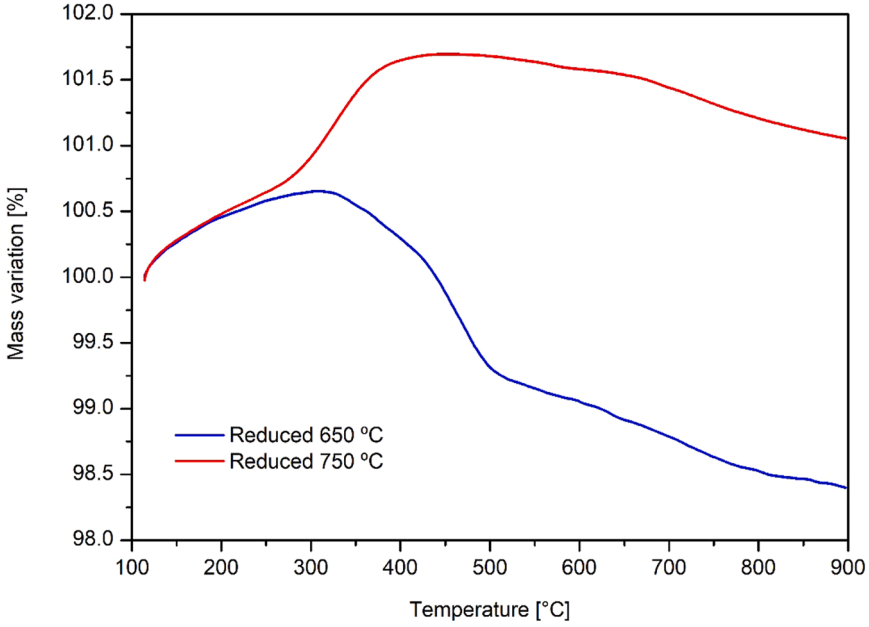

Fig. 8. Weight loss during the oxidation phase in the TGA analyses of the reduced CuO/Al_2O_3 (powder) at 650 °C (Experiment 8) and 750 °C (Experiment 9).

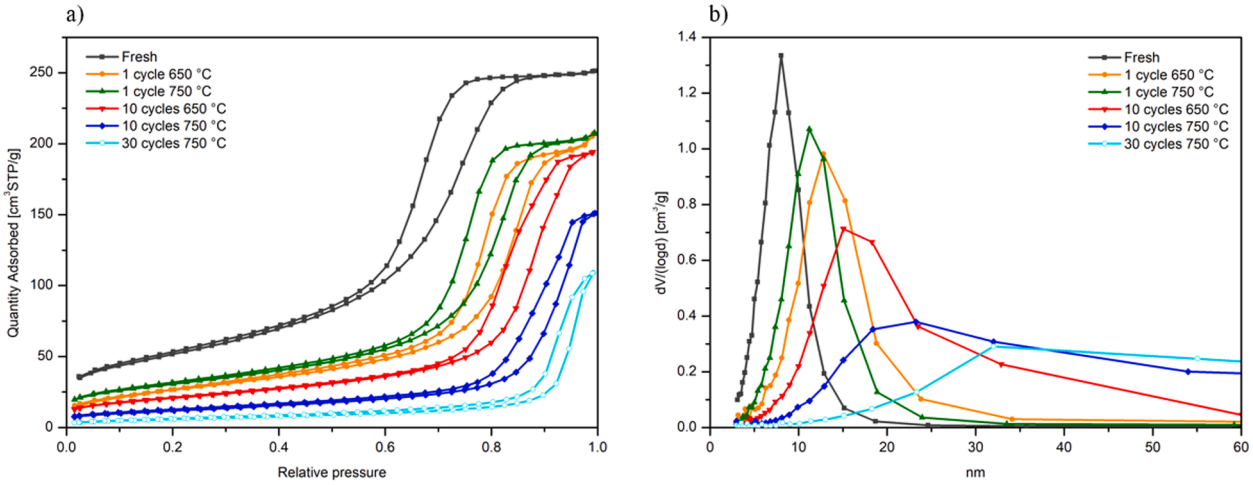

Fig. 9. a) N_2 adsorption-desorption isotherms and b) BJH PSD of the of the CuO/Al_2O_3 powder OC used in this research.

of surface area. At 650 °C (Experiment 7), the OC maintained a high surface area of 108 m^2/g (compared to 158 m^2/g for the fresh sample), yet it exhibited a higher tendency for carbon deposition (1.86 wt%) compared to the run at 750 °C (Experiment 8). This demonstrates that at 650 °C, the process is limited by a kinetic bottleneck were the temperature was insufficient to ensure the complete oxidation of the bio-oil components, regardless of the textural properties. In this regime, the accumulation of unreacted intermediates lead to coke formation. This correlation becomes more evident when analyzing the stability after 10 cycles. A clear divergence in textural evolution was observed: at 650 °C, the surface area dropped to 77 m^2/g, whereas at 750 °C, it suffered a more drastic reduction to 42 m^2/g. Despite having a 45% lower surface area compared to the 650 °C test, the operation at 750 °C remained highly effective, maintaining complete carbon conversion and fully suppressing carbon deposition.

This superior performance, regardless of the specific surface loss, could be explained by two converging factors. First, the higher operating temperature effectively compensates for the reduction in active sites by significantly accelerating both the reaction rates and the oxygen diffusion kinetics within the solid porosity. Second, the average pore diameter increased to 18.4 nm at 750 ºC compared to 15.1 nm at 650 °C after 10 cycles, this fact plays a critical role in mass transfer as the wider pore structure facilitates the diffusion of the compounds into the internal active sites preventing the pore-plugging effects that favor coke formation at lower temperatures.

Finally, the structural integrity of the carrier is supported by the XRD findings. The formation of the $CuAl_2O_4$ spinel phase, which correlates with the increase in crystallite size observed at higher temperatures, acts as a structural stabilizer. This phase prevents the total loss of reactivity and the collapse of the OC framework during repeated redox cycling. Consequently, the CuO/Al_2O_3 OC achieves an optimal balance at 750 °C with wider pores that, combined with enhanced kinetics, and the $CuAl_2O_4$ phase ensures a complete combustion pathway for the complex aqueous bio-oil fraction.

4. Conclusions

The present study demonstrates the feasibility of CLC for the

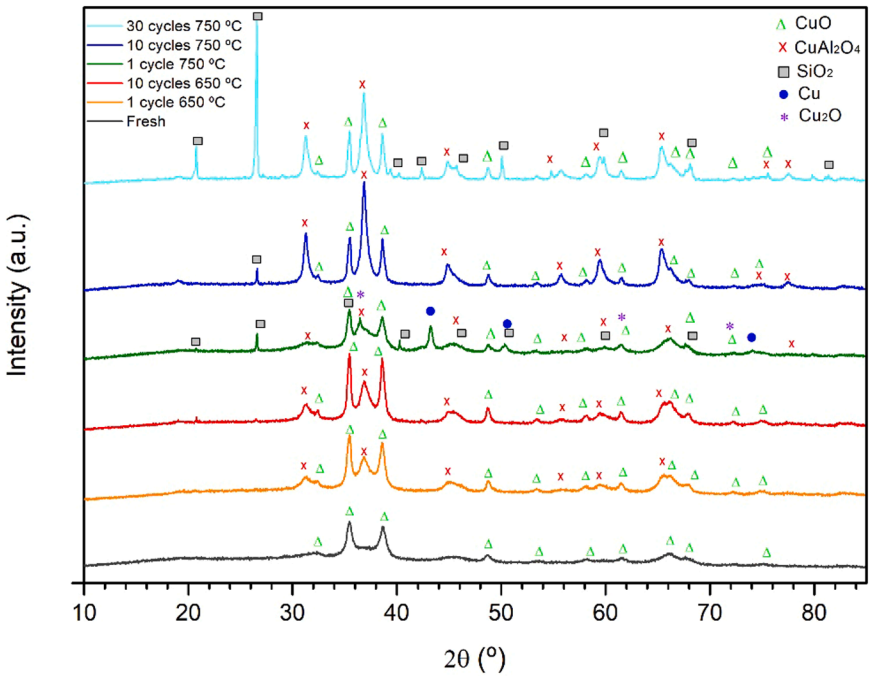

Fig. 10. XRD patterns of the fresh OC, spent in 1 cycle OC at 650 and 750 °C, and spent in multiple cycles OC at 650 (10 cycles), 750 ºC (10 cycles) and 750 °C (30 cycles).

valorization of the aqueous fraction of biomass pyrolysis bio-oil, a complex and low-value waste stream. Using a fixed-bed reactor and a representative synthetic model mixture, the following main conclusions can be drawn:

- **Oxygen carrier screening:** Among the evaluated materials at 650 °C, Cu-based carriers and the Mn-Cu mixed oxide (carulite) showed the highest selectivity towards complete oxidation. The laboratory-synthesized CuO/Al_2O_3 powder exhibited the best overall performance, maintaining complete combustion to CO_2 for the longest period. Conversely, Fe- and Ni-based OCs rapidly transitioned to a reforming-dominated regime, producing significant amounts of H_2, CO, and CH_4 under the tested conditions.
- **Cyclic stability and regenerability:** The CuO/Al_2O_3 demonstrated excellent redox stability and complete regenerability. Extended testing over 30 consecutive cycles (24 h of continuous operation) at 750 °C confirmed that the material maintains its oxygen transfer capacity and reactivity.
- **Carbon management:** Operating temperature played a critical role in carbon formation. While limited carbonaceous deposits were generated on the OC surface at 650 °C (subsequently oxidized during the regeneration step), operation at 750 °C thermodynamically disfavored these side reactions, effectively suppressing coke formation and maximizing the direct conversion of fed carbon to CO_2. Although a minor, constant CO_2 signal was detected during reoxidation in long-term tests, it did not accumulate or interfere with the carrier activity, justifying 750 °C as the optimal condition for the integrated process.
- **Structural evolution:** Long-term operation promoted an increase in crystallinity and the solid-state reaction between CuO and the alumina support, forming a $CuAl_2O_4$ spinel phase, particularly at 750 °C. Although this caused a reduction in the porosity, the overall reactivity and oxygen transfer capacity of the carrier were fully preserved.

Overall, the application of low-temperature CLC using a CuO/Al_2O_3 OC successfully addresses the critical bottlenecks of severe carbon deposition and oxygen carrier deactivation typically associated with bio-oil thermal processing. By mitigating thermal sintering and suppressing coking, this approach provides a robust and practically viable pathway to valorize aqueous bio-oil residues while enabling inherent CO_2 capture.

Despite these promising laboratory-scale results, future work should focus on the following outlook to bridge the gap toward industrial implementation: First, testing real bio-oil fractions is essential to evaluate the long-term impact of impurities (such as sulfur or alkali metals) on carrier poisoning. Second, the mechanical strength and sintering of the CuO/Al_2O_3 particles must be validated. Finally, a detailed techno-economic and life-cycle assessment will be necessary to quantify the energy efficiency gains and the actual carbon footprint reduction of this valorization pathway compared to conventional disposal methods.

CRediT authorship contribution statement

Alejandro Lete: Writing – review & editing, Methodology, Formal analysis, Data curation, Conceptualization. **César Gracia-Monforte:** Writing – review & editing, Writing – original draft, Software, Methodology, Investigation, Formal analysis, Data curation, Conceptualization. **Javier Ábrego:** Writing – review & editing, Validation, Supervision, Project administration, Formal analysis. **Jesús Arauzo:** Writing – review & editing, Supervision, Project administration, Funding acquisition.

Declaration of Competing Interest

The authors declare that they have no known competing financial interests or personal relationships that could have appeared to influence the work reported in this paper.

Acknowledgments

The authors express gratitude for providing frame support for this work to the Project PID2023–1490520B-I00 funded by Agencia Estatal de Investigación and by the European Union. Aragón Government has also given frame support (Research Group Ref. T22_23R). Alejandro Lete extends special thanks to Government of Aragón for its contribution in

the form of a grant for the hiring of predoctoral research staff

Data availability

Data will be made available on request.

References

[1] A. Nandy, C. Loha, S. Gu, P. Sarkar, M.K. Karmakar, P.K. Chatterjee, Present status and overview of Chemical Looping Combustion technology, Jun. 01, Elsevier Ltd, 2016, https://doi.org/10.1016/j.rser.2016.01.003.

[2] Q. Zhang, J. Chang, T. Wang, Y. Xu, Review of biomass pyrolysis oil properties and upgrading research, Energy Convers. Manag 48 (1) (Jan. 2007) 87–92, https://doi.org/10.1016/j.enconman.2006.05.010.

[3] D. Mohan, C.U. Pittman, and P.H. Steele, "Pyrolysis of wood/biomass for bio-oil: A critical review," May 2006. doi: 10.1021/ef0502397.

[4] A.V. Bridgwater, Review of fast pyrolysis of biomass and product upgrading, Biomass Bioenergy 38 (Mar. 2012) 68–94, https://doi.org/10.1016/j.biombioe.2011.01.048.

[5] A. Oasmaa and C. Peacocke, "Properties and fuel use of biomass-derived fast pyrolysis liquids. A guide."

[6] S. Al Arni, Comparison of slow and fast pyrolysis for converting biomass into fuel, Renew. Energy 124 (Aug. 2018) 197–201, https://doi.org/10.1016/j.renene.2017.04.060.

[7] L.R. Santos, D.R. Araujo, M.A.S. Rodrigues, Strategic techniques for upgrading bio-oil from fast pyrolysis: a critical review, . 01, John Wiley and Sons Ltd, 2025, https://doi.org/10.1002/bbb.2789.

[8] S. Conrad, C. Blajin, T. Schulzke, G. Deerberg, Improved fast pyrolysis bio-oils from straw and miscanthus by fractionated condensation, Environ. Prog. Sustain. Energy 41 (1) (Jan. 2022), https://doi.org/10.1002/ep.13708.

[9] S. Czernik, A.V. Bridgwater, Overview of applications of biomass fast pyrolysis oil, Energy Fuels 18 (2) (Mar. 2004) 590–598, https://doi.org/10.1021/ef034067u.

[10] S. Ren, X.P. Ye, Stability of crude bio-oil and its water-extracted fractions, J. Anal. Appl. Pyrolysis 132 (Jun. 2018) 151–162, https://doi.org/10.1016/j.jaap.2018.03.005.

[11] A. Oasmaa, S. Czernik, Fuel oil quality of biomass pyrolysis oils - state of the art for the end users, Energy Fuels 13 (4) (Jul. 1999) 914–921, https://doi.org/10.1021/ef980272b.

[12] M. Ishida, H. Jin, A new advanced power-generation system using chemical-looping combustion, Energy 19 (4) (1994) 415–422, https://doi.org/10.1016/0360-5442(94)90120-1.

[13] J. Adánez, A. Abad, T. Mendiara, P. Gayán, L.F. de Diego, F. García-Labiano, Chemical looping combustion of solid fuels, Mar. 01, Elsevier Ltd, 2018, https://doi.org/10.1016/j.pecs.2017.07.005.

[14] J. Adánez, A. Abad, Chemical-looping combustion: status and research needs, Proc. Combust. Inst. 37 (4) (2019) 4303–4317, https://doi.org/10.1016/j.proci.2018.09.002.

[15] A. Lyngfelt, C. Linderholm, Chemical-Looping Combustion of Solid Fuels - Status and Recent Progress. Energy Procedia, Elsevier Ltd, 2017, pp. 371–386, https://doi.org/10.1016/j.egypro.2017.03.1179.

[16] A. Di Giuliano, S. Capone, M. Anatone, K. Gallucci, Chemical looping combustion and gasification: a review and a focus on European research projects, Oct. 05, American Chemical Society, 2022, https://doi.org/10.1021/acs.iecr.2c02677.

[17] S. Abuelgasim, W. Wang, A. Abdalazeez, A brief review for chemical looping combustion as a promising CO2 capture technology: fundamentals and progress, Apr. 10, Elsevier B.V, 2021, https://doi.org/10.1016/j.scitotenv.2020.142892.

[18] H. Leion, T. Mattisson, A. Lyngfelt, Combustion de charges solides avec la boucle chimique dans un lit fluidisé de laboratoire, Oil Gas. Sci. Technol. 66 (2) (Mar. 2011) 201–208, https://doi.org/10.2516/ogst/2010026.

[19] A. Lyngfelt, Chemical-looping combustion of solid fuels-status of development, 2014.

[20] B. Bhui, P. Vairakannu, Prospects and issues of integration of co-combustion of solid fuels (coal and biomass) in chemical looping technology, Feb. 01, Academic Press, 2019, https://doi.org/10.1016/j.jenvman.2018.10.092.

[21] A. Hoteit, A. Forret, W. Pelletant, J. Roesler, T. Gauthier, Combustion en boucle chimique avec différentes charges liquides, Oil Gas. Sci. Technol. 66 (2) (Mar. 2011) 193–199, https://doi.org/10.2516/ogst/2010022.

[22] F. Güleç, W. Meredith, C.G. Sun, C.E. Snape, Selective low temperature chemical looping combustion of higher alkanes with Cu- and Mn- oxides, Energy 173 (Apr. 2019) 658–666, https://doi.org/10.1016/j.energy.2019.02.099.

[23] P. Moldenhauer, M. Rydén, T. Mattisson, and A. Lyngfelt, "Chemical-looping combustion and chemical-looping with oxygen uncoupling of kerosene with Mn- and Cu-based oxygen carriers in a circulating fluidized-bed 300 W laboratory reactor."

[24] A. Serrano, F. García-Labiano, L.F. de Diego, P. Gayán, A. Abad, J. Adánez, Chemical Looping Combustion of liquid fossil fuels in a 1 kWth unit using a Fe-based oxygen carrier, Fuel Process. Technol. 160 (2017) 47–54, https://doi.org/10.1016/j.fuproc.2017.02.015.

[25] M. Rydén, et al., Chemical-looping combustion with liquid fuels. Energy Procedia, Elsevier Ltd, 2013, pp. 654–661, https://doi.org/10.1016/j.egypro.2013.05.153.

[26] J. Bao, et al., Interaction between Fe-based oxygen carriers and n-heptane during chemical looping combustion, Proc. Combust. Inst. 34 (2) (2013) 2839–2846, https://doi.org/10.1016/j.proci.2012.07.079.

[27] F. Güleç, J.A. Okolie, P.T. Clough, A. Erdogan, W. Meredith, C.E. Snape, Low-temperature chemical looping oxidation of hydrogen for space heating, J. Energy Inst. 110 (Oct. 2023), https://doi.org/10.1016/j.joei.2023.101355.

[28] J. Adanez, A. Abad, F. Garcia-Labiano, P. Gayan, and L.F. De Diego, "Progress in chemical-looping combustion and reforming technologies," Apr. 2012. doi: 10.1016/j.pecs.2011.09.001.

[29] X. Hu, et al., Coke formation during thermal treatment of bio-oil, Energy Fuels 34 (7) (Jul. 2020) 7863–7914, https://doi.org/10.1021/acs.energyfuels.0c01323.

[30] C. Gracia-Monforte, F. Maldonado-Martín, M. Atienza-Martínez, J. Ábrego, Low temperature chemical looping combustion of pyrolysis gases in a fixed bed reactor, Biomass-.-. Bioenergy 199 (Aug. 2025), https://doi.org/10.1016/j.biombioe.2025.107911.

[31] J.C. Maya, F. Chejne, S.K. Bhatia, Effect of sintering on the reactivity of copper-based oxygen carriers synthesized by impregnation, Chem. Eng. Sci. 162 (2017) 131–140, https://doi.org/10.1016/j.ces.2016.12.073.

[32] Q. Imtiaz, A. Armutlulu, F. Donat, M.A. Naeem, C.R. Müller, Preventing Agglomeration of CuO-Based Oxygen Carriers for Chemical Looping Applications, ACS Sustain. Chem. Eng. 9 (17) (May 2021) 5972–5980, https://doi.org/10.1021/acssuschemeng.1c00560.

[33] E. Ksepko, Examining SrCuO2 as an oxygen carrier for chemical looping combustion, J. Therm. Anal. Calor. 122 (2) (Nov. 2015) 621–633, https://doi.org/10.1007/s10973-015-4813-8.

[34] C. Gracia-Monforte, A. Lete, F. Marias, J. Ábrego, J. Arauzo, Energy, exergy and mass balances of a biomass pyrolysis pilot plant, Energy Convers. Manag 353 (Apr. 2026), https://doi.org/10.1016/j.enconman.2026.121154.

[35] A. Lete, R. Raso, L. García, J. Ruiz, J. Arauzo, Synthesis of ketones from glycerol and 1,2-propanediol using copper and nickel catalysts: Unraveling the impact of reaction phase and active metal, Fuel 371 (Sep. 2024), https://doi.org/10.1016/j.fuel.2024.132001.

[36] F. Maldonado-Martín, L. García, J. Ruiz, M. Oliva, J. Arauzo, Selective Conversion of Glycerol to Acetol: Effect of the Preparation Method of CuAl Catalysts and Reaction Phase, Catalysts 15 (4) (Apr. 2025), https://doi.org/10.3390/catal15040348.

[37] S. Conrad, C. Blajin, T. Schulzke, G. Deerberg, Improved fast pyrolysis bio-oils from straw and miscanthus by fractionated condensation, Environ. Prog. Sustain. Energy 41 (1) (Jan. 2022), https://doi.org/10.1002/ep.13708.

[38] I. Adánez-Rubio, et al., Use of Hopcalite-Derived Cu-Mn Mixed Oxide as Oxygen Carrier for Chemical Looping with Oxygen Uncoupling Process, Energy Fuels 30 (7) (Jul. 2016) 5953–5963, https://doi.org/10.1021/acs.energyfuels.6b00552.

[39] P. Cho, T. Mattisson, A. Lyngfelt, Comparison of iron-, nickel-, copper- and manganese-based oxygen carriers for chemical-looping combustion, Fuel 83 (9) (Jun. 2004) 1215–1225, https://doi.org/10.1016/j.fuel.2003.11.013.

[40] S.Y. Chuang, J.S. Dennis, A.N. Hayhurst, S.A. Scott, Development and performance of Cu-based oxygen carriers for chemical-looping combustion, Combust. Flame 154 (1–2) (Jul. 2008) 109–121, https://doi.org/10.1016/j.combustflame.2007.10.005.

[41] A. Abad, J. Adánez, F. García-Labiano, L.F. de Diego, P. Gayán, J. Celaya, Mapping of the range of operational conditions for Cu-, Fe-, and Ni-based oxygen carriers in chemical-looping combustion, Chem. Eng. Sci. 62 (1–2) (Jan. 2007) 533–549, https://doi.org/10.1016/j.ces.2006.09.019.

[42] A. Abad, F. García-Labiano, L.F. de Diego, P. Gayán, J. Adánez, Reduction kinetics of Cu-, Ni-, and Fe-based oxygen carriers using syngas (CO + H2) for chemical-looping combustion, Energy Fuels 21 (4) (Jul. 2007) 1843–1853, https://doi.org/10.1021/ef070025k.

[43] R.R. Davda, J.W. Shabaker, G.W. Huber, R.D. Cortright, and J.A. Dumesic, "A review of catalytic issues and process conditions for renewable hydrogen and alkanes by aqueous-phase reforming of oxygenated hydrocarbons over supported metal catalysts," Mar. 10, 2005. doi: 10.1016/j.apcatb.2004.04.027.

[44] M.M. Hossain and H.I. de Lasa, "Chemical-looping combustion (CLC) for inherent CO2 separations-a review," Sep. 2008. doi: 10.1016/j.ces.2008.05.028.

[45] K.E. Sedor, M.M. Hossain, H.I. de Lasa, Reactivity and stability of Ni/Al2O3 oxygen carrier for chemical-looping combustion (CLC), Chem. Eng. Sci. 63 (11) (Jun. 2008) 2994–3007, https://doi.org/10.1016/j.ces.2008.02.021.

[46] H. Abduhani, et al., Chemical looping gasification characteristics of biomass pyrolysis volatiles with Cu/Ni/olivine oxygen carrier for hydrogen-rich gas, Energy 314 (Jan. 2025), https://doi.org/10.1016/j.energy.2024.134209.

[47] F. Bimbela, M. Oliva, J. Ruiz, L. García, J. Arauzo, Hydrogen production via catalytic steam reforming of the aqueous fraction of bio-oil using nickel-based coprecipitated catalysts, Int. J. Hydrog. Energy 38 (34) (Nov. 2013) 14476–14487, https://doi.org/10.1016/j.ijhydene.2013.09.038.

[48] L.F. de Diego, F. García-Labiano, P. Gayán, J. Celaya, J.M. Palacios, J. Adánez, Operation of a 10 kWth chemical-looping combustor during 200h with a CuO-Al2O3 oxygen carrier, Fuel 86 (7–8) (May 2007) 1036–1045, https://doi.org/10.1016/j.fuel.2006.10.004.

[49] A. Lyngfelt, A. Brink, Ø. Langørgen, T. Mattisson, M. Rydén, C. Linderholm, 11,000 h of chemical-looping combustion operation—Where are we and where do we want to go?, Sep. 01 Elsevier Ltd, 2019 https://doi.org/10.1016/j.ijggc.2019.05.023.

[50] Y. De Vos, M. Jacobs, P. Van Der Voort, I. Van Driessche, F. Snijkers, A. Verberckmoes, Development of stable oxygen carrier materials for chemical looping processes—A review, Aug. 01, MDPI, 2020, https://doi.org/10.3390/catal10080926.

[51] G. Liu, G. Lisak, Cu-based oxygen carriers for chemical looping processes: Opportunities and challenges, Jun. 15, Elsevier Ltd, 2023, https://doi.org/10.1016/j.fuel.2023.127828.

[52] F. Bimbela, M. Oliva, J. Ruiz, L. García, J. Arauzo, Hydrogen production by catalytic steam reforming of acetic acid, a model compound of biomass pyrolysis

liquids (SPEC. ISS), J. Anal. Appl. Pyrolysis 79 (1-2) (2007) 112–120, https://doi.org/10.1016/j.jaap.2006.11.006.
[53] M. Rydén, A. Lyngfelt, T. Mattisson, Synthesis gas generation by chemical-looping reforming in a continuously operating laboratory reactor, Fuel 85 (12–13) (Sep. 2006) 1631–1641, https://doi.org/10.1016/j.fuel.2006.02.004.
[54] H. Zheng, X. Jiang, Y. Gao, A. Tong, L. Zeng, Chemical looping reforming: process fundamentals and oxygen carriers, Dec. 01, Discover (2022), https://doi.org/10.1007/s43938-022-00012-3.
[55] M.T. Izquierdo, et al., On the optimization of physical and chemical stability of a Cu/Al2O3 impregnated oxygen carrier for chemical looping combustion, Fuel Process. Technol. 215 (May 2021), https://doi.org/10.1016/j.fuproc.2021.106740.
[56] M.A. San Pio, M. Martini, F. Gallucci, I. Roghair, M. van Sint Annaland, Kinetics of CuO/SiO2 and CuO/Al2O3 oxygen carriers for chemical looping combustion, Chem. Eng. Sci. 175 (2018) 56–71, https://doi.org/10.1016/j.ces.2017.09.044.
[57] S. Daneshmand-Jahromi, M.H. Sedghkerdar, N. Mahinpey, A review of chemical looping combustion technology: Fundamentals, and development of natural, industrial waste, and synthetic oxygen carriers, Jun. 01, Elsevier Ltd, 2023, https://doi.org/10.1016/j.fuel.2023.127626.
[58] X. Huang, et al., A cost-effective approach to reducing carbon deposition and resulting deactivation of oxygen carriers for improvement of energy efficiency and CO2 capture during methane chemical-looping combustion, Appl. Energy 193 (2017) 381–392, https://doi.org/10.1016/j.apenergy.2017.02.059.
[59] X. Cheng, et al., Enhanced resistance to carbon deposition in chemical-looping combustion of methane: synergistic effect of different oxygen carriers via sequence filling, Chem. Eng. J. 421 (Oct. 2021), https://doi.org/10.1016/j.cej.2021.129776.
[60] P. Cho, T. Mattisson, A. Lyngfelt, Carbon formation on nickel and iron oxide-containing oxygen carriers for chemical-looping combustion, Ind. Eng. Chem. Res. 44 (4) (Feb. 2005) 668–676, https://doi.org/10.1021/ie049420d.
[61] Y. Zhu, K. Mimura, J.-W. Lim, and Q. Jiang, "Brief Review of Oxidation Kinetics of Copper at 350 °C to 1050 °C."
[62] C.H. Bartholomew, Mechanisms of catalyst deactivation, Appl. Catal. A Gen. 212 (1) (2001) 17–60, https://doi.org/10.1016/S0926-860X(00)00843-7.
[63] M.D. Argyle, C.H. Bartholomew, Heterogeneous Catalyst Deactivation and Regeneration: A Review, MDPI, 2015, https://doi.org/10.3390/catal5010145.
[64] A. Lete, F. Lacleta, L. García, J. Ruiz, J. Arauzo, Effect of calcination temperature and atmosphere on the properties and performance of CuAl catalysts for glycerol dehydration to acetol, Biomass Bioenergy 195 (Apr. 2025), https://doi.org/10.1016/j.biombioe.2025.107725.
[65] M. Thommes, et al., Physisorption of gases, with special reference to the evaluation of surface area and pore size distribution (IUPAC Technical Report), Pure Appl. Chem. 87 (9–10) (Oct. 2015) 1051–1069, https://doi.org/10.1515/pac-2014-1117.
[66] A. Alejandre, F. Medina, P. Salagre, X. Correig, J.E. Sueiras, Preparation and study of Cu-Al mixed oxides via hydrotalcite-like precursors, Chem. Mater. 11 (4) (1999) 939–948, https://doi.org/10.1021/cm980500f.